# Quantitative Nanoproteomics for Protein Complexes (QNanoPX) Related to Estrogen Transcriptional Action*[S]

Pai-Chiao Cheng‡, Hsiang-Kai Chang§, and Shu-Hui Chen‡§¶

**We developed an integrated proteomics approach using a chemically functionalized gold nanoparticle (AuNP) as a novel probe for affinity purification to analyze a large protein complex *in vivo*. We then applied this approach to globally map the transcriptional activation complex of the estrogen response element (ERE). This approach was designated as quantitative nanoproteomics for protein complexes (QNanoPX). In this approach, the positive AuNP-ERE probes were functionalized with polyethylene glycol (PEG), and the consensus sequence of ERE and negative AuNP-PEG probes were functionalized with PEG without the ERE via a thiolated self-assembly monolayer technique. The AuNP-ERE probe had substantially low nonspecific binding and high solubility, which resulted in a 20-fold enrichment of the factor compared with gel beads. In addition, the surface-only binding allows the probe to capture a large protein complex without any restrictions due to pore size. The affinity purification method was combined with MS-based quantitative proteomics and statistical methods to reveal the components of the ERE complex in MCF-7 cells and to identify those components within the complex that were altered by the presence of 17$\beta$-estradiol (E2). Results indicated that a majority of proteins pulled down by the positive probe exhibited significant binding, and approximately one-half of the proteins, including estrogen receptor $\alpha$ (ER$\alpha$), were slightly but significantly affected by a 24-h treatment with E2. Based on a combination of bioinformatics and pathway analysis, most of the affected proteins, however, appeared to be related to the transcriptional regulation of not only ER$\alpha$ but also c-Myc. Further confirmation indicated that E2 enhanced the ERE binding of c-Myc by 14-fold, indicating that c-Myc may play a major role, along with ER$\alpha$, in E2-mediated transcription. Taken together, our results demonstrated a successful QNanoPX approach toward new pathway discovery and further revealed the importance of cross-interactions among transcription factors.** ***Molecular & Cellular Proteomics 9:209–224, 2010.***

Estrogen signaling is complex, involving two different isoforms of the estrogen receptor, $\alpha$ (ER$\alpha$)[1] and $\beta$ (ER$\beta$), as well as several different pathways that affect the expression of a number of genes either directly or indirectly. When activated by 17$\beta$-estradiol (E2), the ERs are translocated from the cytosol to the nucleus where the nuclear ERs bind to ERE and recruit other proteins in a complex by promoting, as an activator, or blocking, as a repressor, the recruitment of RNA polymerase to the target genes. The ER·ERE complex controls the transcription of genetic information from DNA to RNA as well as the translation from RNA to proteins. This process, which is known as the genomic pathway, is significantly involved with many diseases, including various cancers. A nongenomic pathway that involves membrane receptors and protein kinases to send the transduction signals to the nucleus has also been described (1, 2). Although there have been studies involving proteomics profiling to identify estrogen-responsive proteins (3, 4), the analysis of protein complexes based on a proteomics approach could provide more insights into specific signaling pathways and cross-interactions, which are rarely explored by other approaches.

In recent years, the analysis of affinity-purified protein complexes in immunoprecipitation (IP) experiments coupled with a proteomics approach using tandem LC-MS/MS for the identification of proteins has become particularly attractive (5, 6). In principle, all the components, even of large complexes, can be identified in a single LC-MS experiment. Furthermore, quantitative proteomics approaches that are based upon stable isotope labeling, when performed along with appropriate control experiments, can distinguish background contamination or nonspecific binding from true interactors or differentiating effects that are caused by different biological states (7–9). Improvements in affinity purification that can be coupled with quantitative proteomics have also been developed, and most of these methods focus on the use of single/dual affinity tags (10, 11) or chemical reactions (12), such as the use of *in vivo* cross-linking agents. In contrast, most of the IP

From the ‡Department of Chemistry and §Institute of Bioinformatics, National Cheng Kung University, Tainan 701, Taiwan

Received, April 13, 2009, and in revised form, September 7, 2009
Published, MCP Papers in Press, October 5, 2009, DOI 10.1074/mcp.M900183-MCP200

[1] The abbreviations used are: ER, estrogen receptor; QNanoPX, quantitative nanoproteomics for resolving protein complexes; AuNP, gold nanoparticle; ERE, estrogen response element; SAM, self-assembly monolayer; E2, 17$\beta$-estradiol; IP, immunoprecipitation; PEG, polyethylene glycol; dsERE, double-stranded ERE; cERE, complementary ERE; NHS, *N*-hydroxysuccinimidyl.

assays are still performed using gel-coupled antibodies (12). These gel beads have high binding capacity because of their porous nature. There are, however, major disadvantages also associated with the porous nature of gel beads composed of agarose or Sepharose. One such disadvantage involves a limitation on the ability of large complexes (13) to diffuse into the pores, which further renders an increase in nonspecific binding as more species could stick on the surface of the beads nonspecifically. Moreover, gel beads can precipitate quickly, which leads to incomplete interactions, even under continuous rotation. The >1-μm size of gel beads necessitates that a minimum quantity of beads be used for each experiment that is typically in the range of 25–50 μl of beads per IP. Monodispersed, superparamagnetic beads (14) in micro or nano sizes are available as a support material that could minimize sample loss and accelerate the processing speed via magnet-assisted separation. Magnetic beads, however, are likely to aggregate, possibly as a result of magnetism or non-homogeneous surface modifications, which therefore leads to incomplete recovery.

Alternatively, gold nanoparticles (AuNPs) can easily be modified with a large selection of functional motifs by the use of self-assembly monolayer (SAM) technology to increase the solubility of the AuNPs, which could greatly improve interfacial interactions. These AuNPs could then be utilized in a variety of applications (15). We previously demonstrated that monodispersed AuNPs are useful for concentrating proteins from a relatively large volume of dilute biological fluids by aggregation. This ability opens up new avenues of research because the traditional TCA precipitation method is ineffective under those conditions (16). Modified AuNPs have been successfully used by other groups for the detection of DNAs (17) and proteins (18) as well as for the fabrication of biosensors. In addition, the surface-only binding of AuNPs imposes no limitation on the size of protein complexes and eliminates the requirement for pore penetration, both of which are useful for IP experiments. Thus, AuNPs have several advantages that can be utilized to develop an efficient affinity purification method. Unlike nanomagnetic beads, AuNPs do need to be separated by centrifugation under conditions that require careful optimization. We investigate the protein-DNA interactome associated with ERE motifs located in the promoter region of a target gene. EREs are known to be regulated by ERα and ERβ, which are transcription factors that bind to the ERE itself. We proposed to functionalize AuNPs with the consensus sequence of ERE using the SAM technique and combine the affinity purification method with stable isotope dimethyl labeling (19–21), statistics, and informatics to identify the pulled down proteins that are associated with the ERE complex. This approach has been designated as quantitative nanoproteomics for protein complexes (QNanoPX). QNanoPX is expected to improve the ways that protein complexes can be analyzed by MS and to help resolve complexes that are related to the transcriptional action of estrogen.

## EXPERIMENTAL PROCEDURES

*Materials and Chemicals*—$HAuCl_4 \cdot 3H_2O$ was purchased from Alfa Aesar (Johnson Matthey Co., London, UK). Thiolated polyethylene glycol (HS-PEG) and amine-modified polyethylene glycol ($NH_2$-PEG) with molecular weight 750 were obtained from Rapp Polymere GmbH (Tübingen, Germany). Thiolated DNA containing the ERE sequence (HS-$T_{25}$ERE) (HS-5′-$T_{25}$-GGTCAGAGTGACC-3′), amine-modified DNA with the ERE sequence ($NH_2$-$T_{25}$ERE) ($NH_2$-5′-$T_{25}$-GGTCA-GAGTGACC-3′), and their complementary sequences without (cERE) (5′-GGTCACTCTGACC-3′) and with Cy5 modification (Cy5-cERE) (Cy5–5′-GGTCACTCTGACC-3′) were synthesized by MDBio, Inc. (Taipei, Taiwan). Antibodies against human ERα were purchased from Santa Cruz Biotechnology, Inc. (Santa Cruz, CA), antibodies against TIF1β and c-Myc were from Cell Signaling Technology (Beverly, MA), and antibodies against AN32A and BZW1 were purchased from Abnova (Taipei, Taiwan). The secondary antibody was from Jackson ImmunoResearch Laboratories. Sequence grade modified trypsin was from Promega (Madison, WI), and the E2 compound was from Sigma. The following buffers were prepared: binding buffer, which contains 10 mM Tris, 50 mM NaCl, and 1 mM EDTA at pH 7.5; PBST buffer, which contains 0.05% Tween 20 in PBS buffer; radioimmunoprecipitation buffer, which contains 1% Nonidet P-40, 0.5% sodium deoxycholate, and 0.1% SDS with 0.5 mM PMSF, 1 mM sodium orthovanadate, and 25 μg/ml leupeptin; lysis buffer, which contains 10 mM HEPES, 10 mM KCl, 0.5 mM EDTA, 0.5 mM EGTA, 1 mM DTT, 0.5 mM PMSF, 1 mM sodium orthovanadate, and 25 μg/ml leupeptin at pH 7.9; and nuclear buffer, which contains 20 mM HEPES, 10 mM KCl, 1 mM EDTA, 1 mM EGTA, 1 mM DTT, 0.5 mM PMSF, 1 mM sodium orthovanadate, and 25 μg/ml leupeptin.

*Probe Fabrication*—AuNPs, at a concentration of ~10 nM, were prepared by sodium citrate reduction following the procedures reported earlier (16). For the fabrication of the AuNP-PEG negative probe, a volume of 10 μl of 500 μM HS-PEG (molecular weight, 750) was added to 1 ml of synthesized AuNPs. After an overnight incubation at 4 °C, the negative probe was washed and resuspended in PBS. For the fabrication of AuNP-ERE positive probes, double-stranded ERE (dsERE) was first prepared by mixing 5 μl of 500 μM HS-$T_{25}$ERE and 5 μl of 500 μM complementary ERE (cERE) in 60 μl of binding buffer for the hybridization reaction. After heating at 90 °C for 4 min, the solution was cooled slowly to 40 °C for 20 min, and the formation of dsERE was confirmed by agarose gel electrophoresis (Fig. S1 in Supplement 1). The solution containing the HS-dsERE and 1 μl of 500 μM HS-PEG (0.2:1 for PEG:ERE) was then added to 1 ml of the AuNP solution, and the mixture was incubated for 2 h at room temperature. Sodium chloride was added to a final concentration of 0.1 M. After overnight incubation at 4 °C, the fabricated probes were washed and resuspended in PBS buffer. Gel-PEG negative probe was fabricated by adding 10 μl of 500 μM $NH_2$-PEG into 1 ml of gel-NHS (*N*-hydroxysuccinimidyl-agarose, Sigma), which was resuspended in PBS buffer. The mixture was continuously rotated overnight at 4 °C. For the fabrication of the positive gel-ERE probes, a volume of 60 μl of the solution containing $NH_2$-dsERE and $NH_2$-PEG at a PEG:ERE molar ratio of 0.2:1 was added to 1 ml of gel-NHS solution, and the mixture was rotated for 2 h at room temperature. Sodium chloride was added to a final concentration of 0.1 M. After an overnight reaction at 4 °C, the fabricated probes were washed and resuspended in PBS buffer. Gel electrophoresis, UV-visible spectroscopy, dynamic light scattering, and fluorescence titration were used to characterize the homogeneity and the size of the probe as well as the number of bound ERE molecules on the probe. These procedures are described in Supplement 1.

*Cell Culture and Nuclear Extraction*—Human breast cancer cells (MCF-7) were cultured in phenol red-free Dulbecco's modified Eagle's medium (Sigma) that was supplemented with 10% fetal bovine serum

(Invitrogen), 17.8 mM $NaHCO_3$, and 1% antibiotic-antimycotic (Invitrogen) at pH 7.2. Cells were grown in a 37 °C humidified incubator containing 5% $CO_2$ until confluence. For E2 treatment, the cells were starved for 18 h followed by the addition of E2 to reach a final concentration of $10^{-8}$ M. The solution was then incubated for 24 h at 37 °C. After washing with PBS, the cells were collected using a volume of 200 μl of radioimmunoprecipitation buffer/10-cm dish. The collected cells were lysed for 2 h by gentle rotation at 4 °C. After centrifugation at 13,800 × *g* for 15 min at 4 °C, the supernatant, containing the whole cell lysate, was carefully collected. For nuclear extraction, the cells were washed with PBS buffer after a 24-h treatment and then collected with trypsin. After washing with ice-cold PBS two to three times, the pellets were resuspended in a 10× cell volume of lysis buffer followed by continuous rotation of the solution for 15 min at 4 °C. This sample was then centrifuged at 1000 × *g* for 15 min at 4 °C to separate the nuclear from the non-nuclear fraction. The pellet was resuspended with a 10× cell volume of the nuclear buffer, and the solution was continuously rotated for 2 h at 4 °C. The resulting supernatant contained the nuclear extract.

*Affinity Purification Assay*—A 100-μl volume of the probe solution was diluted with PBS buffer up to a 1-ml total volume and then incubated with the cell lysate containing 100 μg of total protein overnight at 4 °C. After a PBST wash, the pulled down proteins were boiled with the loading dye and directly loaded onto a 10% SDS-polyacrylamide gel for Western blotting. In addition, the pulled down proteins were also eluted by 1% SDS followed by stable isotope dimethyl labeling, TCA precipitation, trypsin digestion, and HPLC fractionation for analysis by LC-MS/MS for protein identification.

*Western Blotting Analysis*—After electrophoresis, the separated proteins were transferred to a 0.22-μm PVDF membrane (Stratagene, La Jolla, CA). The membrane was first blocked with 5% nonfat milk and then incubated with the primary antibodies followed by the secondary antibodies. The blot was developed using an enhanced chemiluminescence detection reagent (Amersham Biosciences ECL Plus, GE Healthcare), and the spot intensity was digitized using a computerized image analyzer (UVP, Upland, CA).

*Trypsin Digestion and Dimethyl Labeling*—The pulled down proteins were first reduced with 10 mM DTT and 1% SDS and boiled for 5 min. The resulting free cysteine residues were alkylated with 50 mM iodoacetamide at room temperature in the dark for 30 min. The salts were removed by TCA precipitation, and the pellet was digested with trypsin at an enzyme to protein ratio of 1:100 in 100 mM ammonium bicarbonate, pH 8 at 37 °C for 18 h. Stable isotope dimethyl labeling was performed as described before (19) for comparative quantification. Briefly, the tryptic peptides were dissolved in 100 mM sodium acetate buffer, pH 5–6 and then added to 5 μl of $H_2$- or $D_2$-formaldehyde (4% in water) and 5 μl of freshly prepared 600 mM sodium cyanoborohydride. After vortexing, this mixture was allowed to react for 10 min, and after the reaction, 5 μl of ammonium hydroxide (7% in water) was added to quench the unreacted formaldehyde. The tryptic digest of the eluted proteins from the AuNP-ERE and the AuNP-PEG probe were labeled with $D_2$- or $H_2$-formaldehyde, respectively, and the combined mixture was then injected into a HPLC system (Model L-7100, Hitachi, Tokyo, Japan) equipped with UV detection and a $C_{18}$ column (VYDAC, 5-μm inner diameter, 300-Å pore size, 4.6 × 250 mm) for fractionation. Mobile phase A consisted of 0.1% TFA in 98% acetonitrile solution, and mobile phase B consisted of 0.1% TFA in 2% acetonitrile solution. The elution gradient was as follows: 0–10 min, 100% B; 10–40 min, 100–80% B; 40–80 min, 80–60% B; 80–100 min, 60–40% B; 100–110 min, 40–10% B; 110–125 min, 10–100% B; and 125–130 min, 100–100% B at a flow rate of 1 ml/min. The collected fractions were dried by vacuum and redissolved in a buffer composed of 2% ACN and 0.1% formic acid.

*Nano-LC/MS Analysis*—The ESI-MS data were obtained using a Q-TOF micro instrument (Micromass, Manchester, UK) equipped with a nanoflow HPLC system (LC Packings, Amsterdam, Netherlands). A 25-μl sample fraction was injected, concentrated by a $C_{18}$ nanoprecolumn cartridge (300-μm inner diameter × 1 mm, 5-μm $C_{18}$, P/N160458, LC Packings), and then separated by a $C_{18}$ column (75-μm inner diameter, 280-μm outer diameter × 15 cm, 3-μm $C_{18}$, LC Packings). Mobile phase A consisted of 0.1% formic acid in 5% acetonitrile solution, and mobile phase B consisted of 0.1% formic acid in 80% acetonitrile solution; a linear gradient from 5 to 90% B over a 90-min period at a flow rate of 250 nl/min was applied. For identification, the MS/MS spectra were obtained by performing survey scans; the MassLynx 4.0 Global ProteinLynx software was used to produce the peak list from raw data, and all sequential scans with the same precursor were combined. The survey scan was from *m/z* 400 to 1600, and the MS/MS scan was from *m/z* 50 to 2000. A Quality Assurance score of 10 was used to filter MS/MS signals with poor quality, and the settings to generate the pkl files were as follows: background subtraction using a polynomial order of 15 and 20% peak curve, peak smoothing using Savitzky-Golay mode with 3.00 channels and two smooths, and peak centroid using a minimum of four peak widths at half-height and 80% centroid top. Proteins were identified using the in-house MASCOT v2.2.1 search engine on the Swiss-Prot 51.6 (human) protein database (257,964 sequences; 15,720 human protein sequence entries). The false positive rate was determined by searching on a reversed protein database and calculated automatically by choosing the "decoy" function from MASCOT web site. The mass tolerance was set to be 0.2 Da for precursor and 0.2 Da for product ions. Dimethyl (Lys), dimethyl (N terminus), dimethyl:2H(4) (Lys), and dimethyl:2H(4) (N terminus) were chosen as variable modifications; carbamidomethyl (Cys) was chosen as a fixed modification; and one missed cleavage on trypsin was allowed. We set the cutoff score to 20 to eliminate low score peptides, and only "rank1" (best match for each MS/MS) peptides were included. Only proteins within the significant hit lists ($p < 0.05$) were regarded as identified proteins. Under these criteria, the cutoff score is 37 and 20 for proteins and peptides, respectively. Manual inspections to exclude false identifications and a reversed database search for the false identification rate were further performed.

For quantification, in-house software specifically designed for quantifying dimethylated peptides was applied. All of the spectra containing both mass peaks of $D_4$- and $H_4$-labeled peptides were combined to produce a composite MS spectrum. The ratios of the $D_4$- and $H_4$-labeled peptides in the composite MS spectra were calculated from the sum of the peak heights of the first three isotopic peaks. The quantification ratio of proteins was calculated by averaging the intensity ratios of peptide ions that matched to the same protein, and a Q test was applied to discriminate outliers.

*Biostatistics*—Quantitative data deduced from the pulldown by the positive ($D_4$) and the negative ($H_4$) probe from the total lysate of MCF-7 cells as well as those identified from the nuclear fractions with and without E2 treatment were evaluated by the Student's *t* test (22) using the free software R Package to decide whether each protein quantification ratio significantly differed from the control protein (BSA) within a stated confidence level.

## RESULTS

*AuNP-ERE Probes*—As depicted in Fig. 1*A*, the AuNP-ERE probe was fabricated by modifying the surface of AuNPs with HS-PEG (molecular weight 750) and dsERE molecules. The bare AuNP was characterized with an approximate diameter of 19.2 nm in hydrated form and increased to 22.5 and 25.9 nm for the negative (AuNP-PEG) and positive (AuNP-ERE)

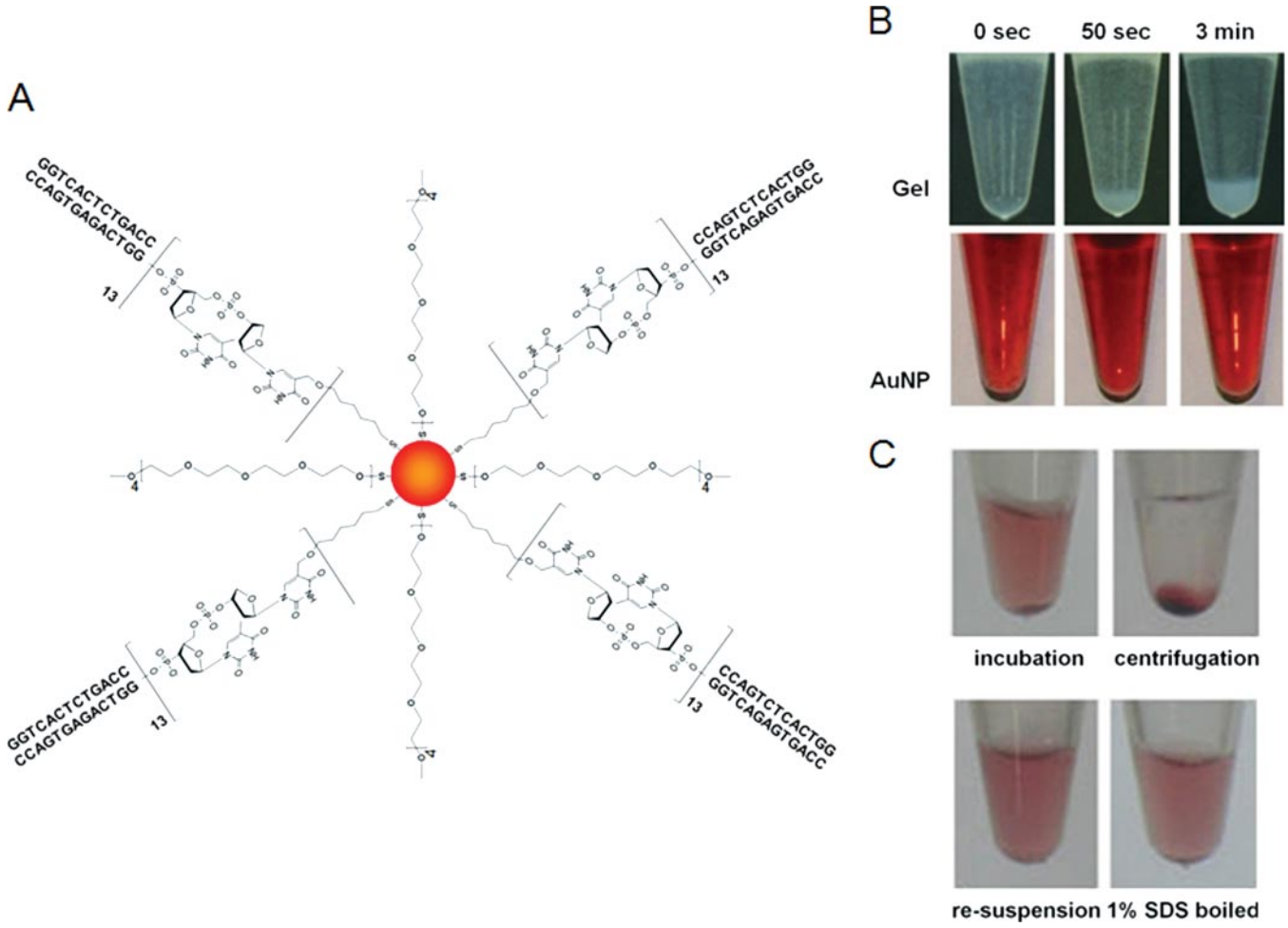


FIG. 1. *A*, molecular scheme of the AuNP-ERE probe. *B*, suspension and precipitation of the AuNPs and gel probes. *C*, centrifugation and redispersion of the pulldown for affinity purification.

probes, respectively, as determined by dynamic light scattering (Table S1 in Supplement 1). Fluorescence titration (Fig. S5 in Supplement 1) revealed that there were an estimated seven ERE molecules bound to one AuNP-ERE probe, and the modification was complete (near 100% yield) and homogeneous as indicated from gel electrophoresis (Fig. S3 in Supplement 1).

Compared with gel beads, AuNP probes have a much higher solubility, which could potentially enhance any interfacial interactions. Although gel beads easily precipitate when incubated for a period longer than 50 s (Fig. 1*B*), the modified AuNP probes remain suspended, as indicated by the *red* color, for months. These suspended AuNPs can also be collected by centrifugation and easily redispersed in an SDS elution buffer that denatures proteins and releases them from the AuNPs (Fig. 1*C*).

The ability of the AuNP-ERE probe for affinity capture of its binding factors was investigated through affinity purification. ER$\alpha$ was pulled down from the recombinant protein solution with no detectable amount left in the supernatant (Fig. 2*A*). Moreover, the amount of ER$\alpha$ that was eluted from the AuNP-ERE probe increased with the percentage of SDS with the recovery yield estimated to be greater than 80% at 1% SDS. The eluted proteins were digested and identified as ER$\alpha$ by its four tryptic peptides via MS/MS sequencing (Supplement 2) with a representative spectrum of the tryptic peptide, GEVGSAGDMR, shown in Fig. 2*B*.

The nonspecific binding and loading capacities associated with AuNPs were compared with those of the gel beads through an examination of the ratio of highly abundant proteins, which are likely to bind nonspecifically to ER$\alpha$ pulled down by the probes. Using equivalent amounts of MCF-7 cell lysate (100 $\mu$g) and probe volume (100 $\mu$l), Coomassie Blue staining indicates that many more nonspecifically binding proteins were pulled down by the negative gel-PEG probe than by the negative AuNP-PEG probes (Fig. 3*A*). The positive gel-ERE probe also appeared to have more nonspecific binding than the positive AuNP-ERE probe. The data from the ER$\alpha$ Western blot analyses also indicate that a lot more ER$\alpha$ was pulled down nonspecifically by the negative gel-PEG probe than by the negative AuNP-PEG probe (Fig. 3*B*). The loading capacity was calculated by subtracting the amount of ER$\alpha$

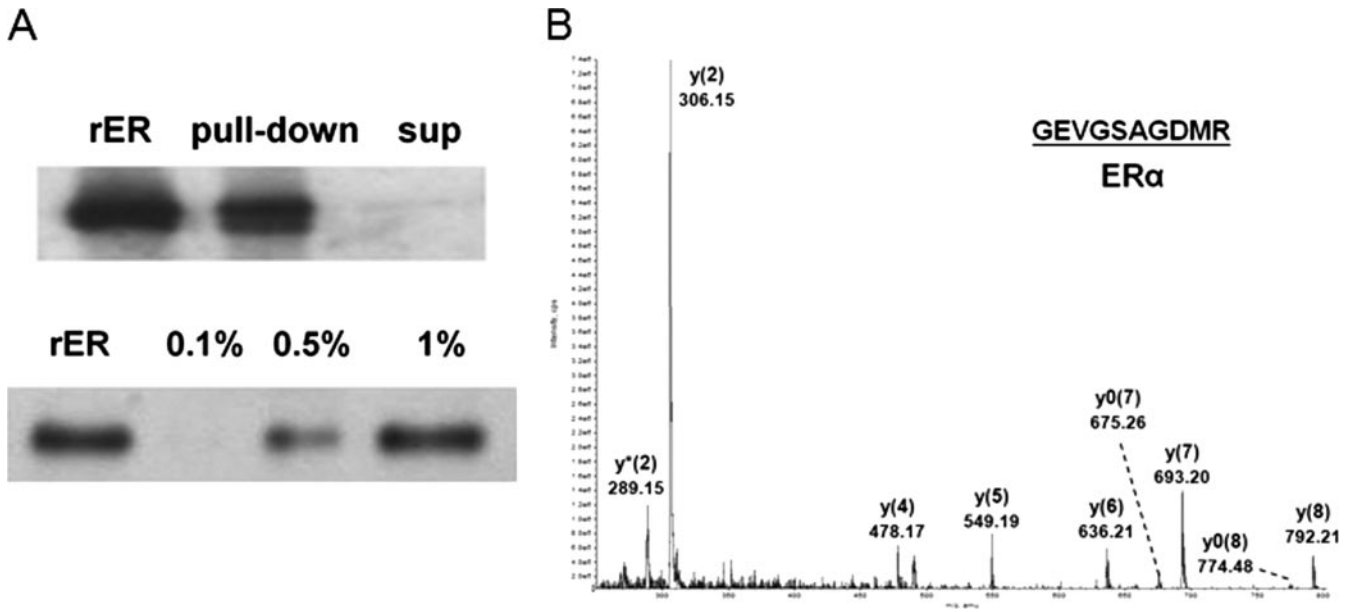


FIG. 2. **Affinity capture of ERα by the AuNP-ERE probe from 0.15 ng/μl recombinant ERα (*rER*) solution.** *A*, the pulldown and supernatant (*sup*) detected without elution or detected after elution from AuNPs by various compositions of SDS buffer. *B*, MS/MS spectra of the tryptic peptide, GEVGSAGDMR, derived from the eluted ERα.

pulled down by the negative probe from the amount pulled down by the positive probe, and no significant differences in the loading capacity between the AuNP-ERE and gel-ERE probes ($p > 0.05$) (Fig. 3*B*) were found. The enrichment factor was calculated by dividing the amount of ERα pulled down by the positive probe by the amount pulled down by the negative probe. The enrichment factors for the AuNP probe and the gel probe were 22 ± 2 and 1.2 ± 0.4, respectively (Fig. 3*B*), which indicated that the substantial nonspecific binding greatly degraded the enrichment factor for the gel probe despite the similar loading capacity.

*Protein Identification and Quantification*—Two stable isotope dimethyl labeling-coupled pulldowns were performed to investigate two features (Fig. 4, *A* and *B*): 1) the specific/nonspecific binding from the total cell lysate by using positive (AuNP-ERE) and negative (AuNP-PEG) probes and 2) E2-induced changes in protein expression within the nucleus by using the AuNP-ERE probe. For Experiment 1, the pulldowns by the negative and the positive probes from the total cell were labeled with $H_4$-formaldehyde and $D_4$-formaldehyde, respectively. A total of 303 proteins were identified and quantified with a low false identification rate of peptides (less than 2.51%). The MS/MS spectra of peptides derived from TIF1β, AN32A, and BZW1, respectively, are shown in Fig. 5*A*. The enhanced $a_1$ ion mass tag of dimethylated peptides was used for fingerprinting to determine the identity of the N-terminal amino acid; this greatly increases the confidence in identifying a protein (20). Thus, in addition to the cutoff score of 20, proteins identified by a single peptide must have an enhanced dimethylated $a_1$ ion in the MS/MS spectrum. For Experiment 2, the pulldown from the nuclear fraction of cells without E2 treatment was labeled with $H_4$-formaldehyde, and the pulldown from the nuclear fraction of cells with a 24-h E2 treatment was labeled with $D_4$-formaldehyde. A total of 250 proteins were identified and quantified with a false identification rate of less than 4.19%. A total of 84 proteins were identified and quantified in both Experiments 1 and 2. A detailed list of these identified proteins is provided in Supplement 2.

The ratio distributions obtained from the two experiments are displayed in Fig. 4, *C* and *D*, respectively. Serum albumin, with calculated ratios of 1.0 ± 0.6 ($n = 15$) and 0.8 ± 0.0 ($n = 2$) for Experiments 1 and 2, respectively, was used as the control to examine whether the protein ratio differs significantly compared with the control. In Experiment 1, 90 and 75% (one tail) was used as the cutoff confidence level, and a ratio value of 2.0 was used as the cutoff for significant binding for proteins that were quantified by a single peptide. For Experiment 2, 75% (two tails) was used as the cutoff confidence level, and values of 1.3 and 0.6 were used as the high and low end cutoffs, respectively, for proteins that were quantified by a single peptide. A detailed list of quantification ratios for all identified proteins is given in Supplement 3. A total of 236 and 147 proteins were found to have quantification ratios that significantly differed from those of the control for Experiments 1 and 2, respectively. Among these proteins, 43 proteins, including ERα, were determined to have significant binding (Experiment 1) as well as significant changes under E2 stimulation (Experiment 2).

The enrichment factors of TIF1β, AN32A, and BZW1, as indicated from their ratio values in pulldowns by the positive and negative probes, were further validated by Western blotting. Among the three proteins, AN32A and BZW1 were quan-

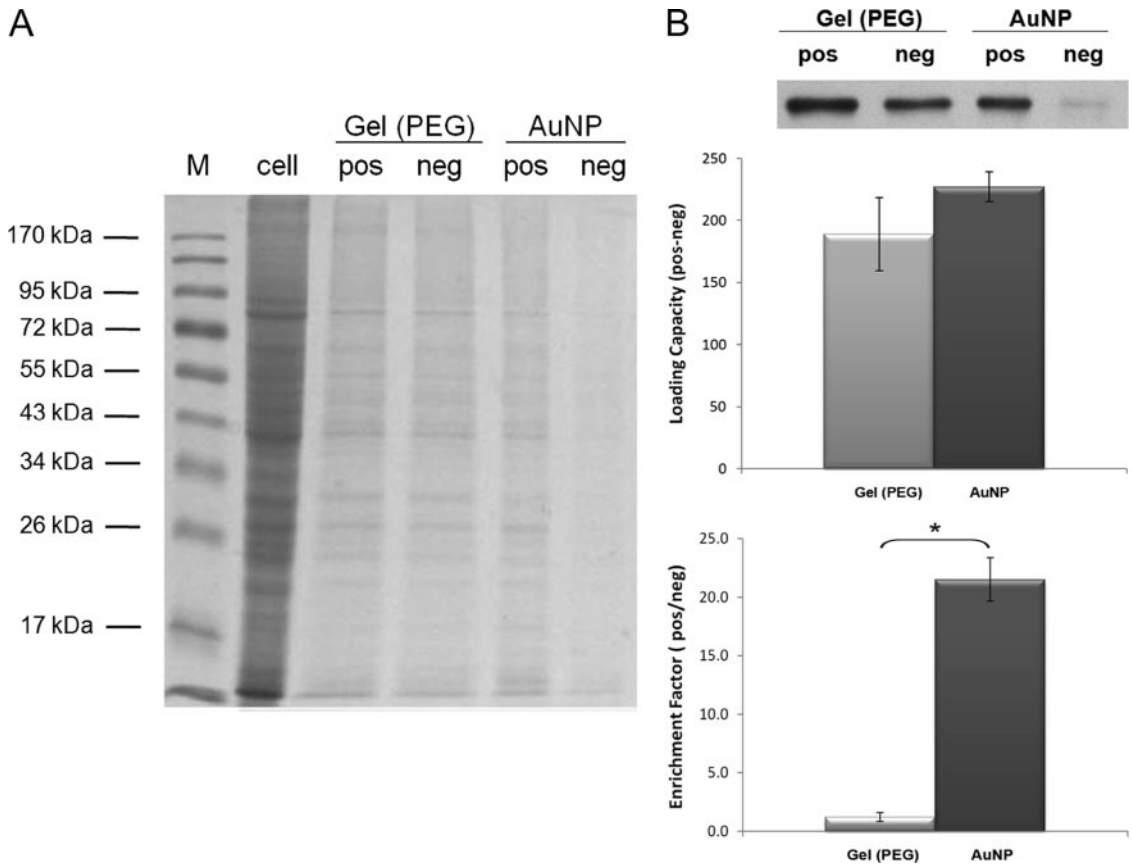


FIG. 3. **The pulldown from MCF-7 cells (100 $\mu$g of total protein) by 100 $\mu$l of AuNP-ERE and gel-ERE probe (positive and negative probes, respectively).** *A*, nonspecific binding proteins of both probes were revealed by 10% SDS-PAGE stained with Coomassie Blue. "*M*" and "*cell*" *lanes* were loaded with protein marker and the total cell lysate without pulldown, respectively. *B*, ER$\alpha$ blotting data for the pulldowns. The loading capacity and enrichment factor were calculated by taking the difference and the ratio between the two pulldowns from the positive (*pos*) and negative (*neg*) probes. There is no significant difference in loading capacities ($n = 3$, $p > 0.05$), but there is a significant difference in enrichment factors ($n = 3$, $p < 0.05$). Significant differences are indicated with the star *, $p < 0.05$.

tified by a single peptide. The ratio value for TIF1$\beta$ was calculated to be 2.8 $\pm$ 1.1 ($n = 7$) based on the MS chromatogram in contrast to the value of 4.4 $\pm$ 1.2 ($n = 3$) deduced from the blotting data (Fig. 5*B*). The ratio value for AN32A was calculated to be 8.0 ($n = 1$) from the MS chromatogram in contrast to the value of 8.0 $\pm$ 2.4 ($n = 3$) deduced from the blotting data. Finally, the ratio value for BZW1 was calculated to be 6.3 ($n = 1$) from the MS chromatogram in contrast to the value of 5.6 $\pm$ 2.0 ($n = 3$) deduced from the blotting data. This general trend of the ratio values was consistent with no significant differences ($p > 0.05$) between the two quantification methods, even for those proteins that were identified by a single peptide.

*Bioinformatics Analysis of the ERE Protein Complex*—Because a majority of the proteins pulled down in Experiment 1 were determined to be significantly bound, those proteins that were identified in Experiment 2 were all assumed to be significantly bound. Thus, the ratio value was then used to indicate the effect of E2 on the levels of protein expression. A bioinformatics analysis was performed to characterize the functional role of 236 proteins with significant binding from Experiment 1 and all 250 proteins identified from Experiment 2. Proteins identified from Experiments as suggested were classified into nine categories according to their functions: transcription factor and coactivators (5 and 4%), transcription or mRNA processing (5 and 11%), translation (8 and 14%), signal transduction (4 and 6%), heat shock protein (4 and 8%), cell cycle (16 and 6%), metabolism (25 and 12%), transport (7 and 7%), structure (15 and 16%), and others (11 and 16%). Apparently, more transcription- and translation-related proteins and fewer cell cycle- and metabolism-related proteins were pulled down from the nuclear fraction (Experiment 2) than from the total cell lysate (Experiment 1).

The 147 proteins (Table I) that showed significant changes induced by a 24-h E2 treatment from Experiment 2 were further annotated by pathway analysis using Metacore software (GeneGo Pathway Analysis, Inc.). The resulting pathway map is shown in Fig. S6 of Supplement 1, and it strongly suggests that almost all of these proteins are involved in transcriptional regulation via transcription factor ER$\alpha$ or c-Myc. Moreover, as indicated in Table I, half of them (75 proteins) are affected by both ER$\alpha$ and c-Myc.

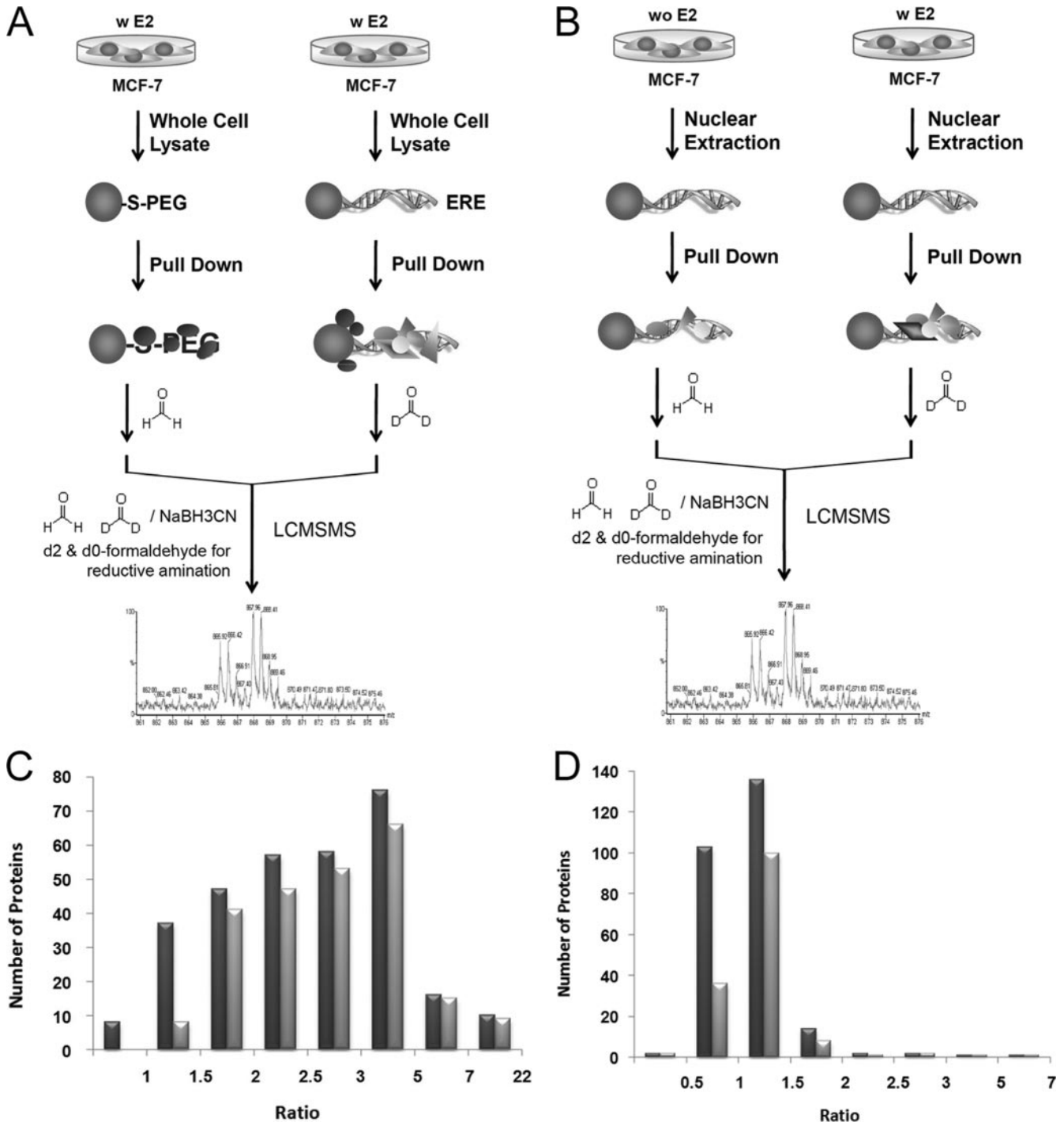


FIG. 4. *A*, schematics of Experiment 1 for specific/nonspecific binding using the positive and negative probes. *B*, schematics of Experiment 2 for the nuclear fractions of MCF-7 cells with (*w*) and without (*wo*) a 24-h E2 treatment using the positive probe. *C*, distribution of all ratios (*black*) and ratios that indicate significant differences (*gray*) compared with the control from Experiment 1. *D*, distribution of all ratios (*black*) and ratios that indicate significant differences (*gray*) compared with the control from Experiment 2.

*E2-induced Changes in ERα and c-Myc by Western Blotting*—Western blotting on ERα and c-Myc was then performed to confirm their functional involvement in the ERE complex as implied by QNanoPX and bioinformatics analysis. First of all, the translocation of ERα from the cytosol to the nucleus upon 24-h E2 treatment was investigated. As shown in Fig. 6, the 24-h E2 treatment caused a reduction of total ERα expression by nearly 20% (Fig. 6*A*; $p < 0.05$). E2 treatment, however, caused the percentage of ERα in the nuclear fraction to increase from 70 to 90%, and ERα in the non-

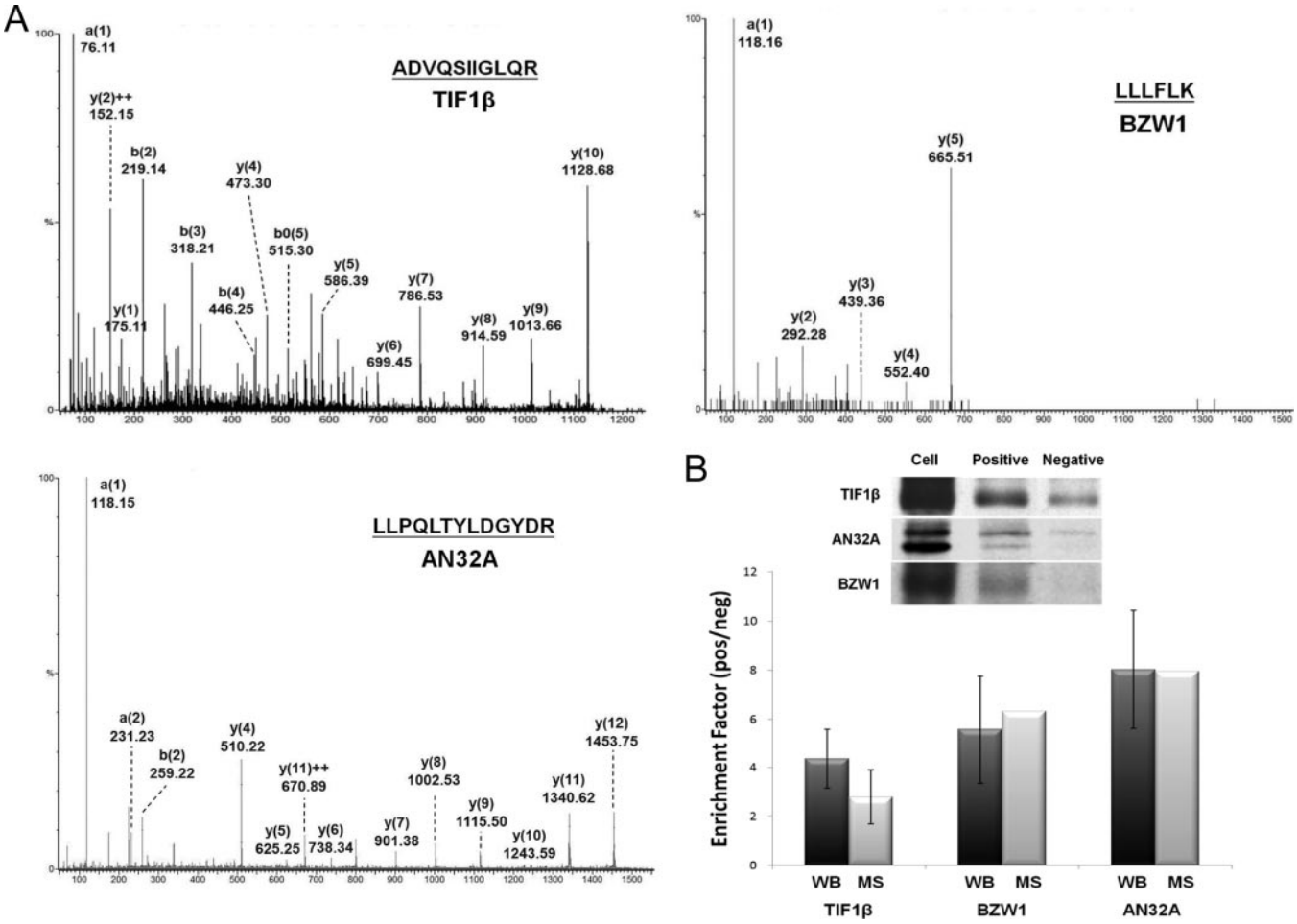


FIG. 5. *A*, representative MS/MS spectra of the tryptic peptides derived from the pulled down proteins (TIF1$\beta$, AN32A, and BZW1) from MCF-7 cells. Enhanced $a_1$ ions were detected in all spectra. *B*, the enrichment factor (ratio values) obtained from stable isotope dimethyl labeling (*open*) and from Western blotting (*WB*) (*black*). No significant differences between the two methods were found for all three proteins ($n = 3$, $p > 0.05$).

nuclear fraction decreased from 30 to 10% (Fig. 6*B*; $p < 0.05$). Thus, the amount of ER$\alpha$ bound to ERE is expected to increase by E2 treatment. Data shown in Fig. 6*C* indicate that the ratio of ER$\alpha$ pulled down from the nucleus with and without E2 treatment is near $0.9 \pm 0.1$, which indicates a slight but significant increase of ER$\alpha$ pulled down with a 24-h E2 treatment compared with the ratio of $0.8 \pm 0.0$ for the control (serum albumin). Compared with ER$\alpha$, the E2-induced change for c-Myc was much more dramatic. As shown in Fig. 6*D*, E2 enhanced c-Myc binding to ERE by a factor of nearly 14. These results confirm the transcriptional involvement of both ER$\alpha$ and c-Myc and further revealed that c-Myc may play a major role in the transcriptional action of estrogen.

## DISCUSSION

*AuNP-ERE Probes for Affinity Pulldown*—The SAM technique used to modify the surface of AuNPs is highly important for affinity purification and critically affects the quality of the results. In our design, the capture molecule (HS-$T_{25}$ERE) has a longer chain and is spaced by a shorter PEG molecule (molecular weight, 750) to minimize the steric hindrance for the complex. Meanwhile, the shorter PEG molecule was used to reduce nonspecific binding due to its hydrophilic and neutral nature. Porous gel beads, on the other hand, could easily attract nonspecific binding proteins due to not only polar functional groups on their surface but also porous structures that make it easy for molecules to stick and hard to escape. Compared with porous gels, the surface-only binding of AuNPs provides no size exclusion for protein complexes, and the pulldown time may also be reduced. On the other hand, the large surface area associated with AuNPs gives them comparable loading capacity with the porous microgels (Fig. 3*B*). Based on the calculation, for seven ERE molecules per AuNP with a hydrated diameter around 26 nm, the loading capacity was estimated to be around 500 kg/m$^3$ for ER$\alpha$ (66 kDa), which is indeed about the same order of magnitude compared with the reported value (180 kg/m$^3$) for BSA on porous Sepharose (23).

TABLE I

*ERE complex proteins with significant changes after a 24-h E2 stimulation*

Proteins marked in bold were identified by both Experiments 1 and 2. TR, transcription regulation; B, binding; SDR, short-chain dehydrogenases/reductases; TRAP, thyroid hormone receptor-associated protein; UBX, domain present in ubiquitin-regulatory proteins; —, not applicable.

| Swiss-Prot accession no. | Protein name | Mean ± S.D. | No. of peptides | Molecular mass | Comments | Refs. |
|---|---|---|---|---|---|---|
| | | | | *Da* | | |
| **1. Only ERα-related** | | | | | | |
| Q9NXB9 | Elongation of very long chain fatty acids protein 2 | 0.957 ± 0.054 | 2 | 34,803 | TR | 25 |
| Q96JQ0 | Protocadherin-16 precursor | 1.333 | 1 | 346,712 | TR | 26 |
| **Q14980** | **Nuclear mitotic apparatus protein 1** | **0.599** | **1** | **239,214** | **TR** | **27** |
| P19012 | Keratin, type I cytoskeletal 15 | 1.006 ± 0.113 | 19 | 49,365 | TR | 27 |
| **P08727** | **Keratin, type I cytoskeletal 19** | **1.102 ± 0.237** | **155** | **44,065** | **TR** | **25** |
| **2. Only c-Myc-related** | | | | | | |
| **P62081** | **40 S ribosomal protein S7** | **1.200 ± 0.116** | **4** | **22,113** | **TR** | **26** |
| **P08195** | **4F2 cell surface antigen heavy chain** | **0.905 ± 0.002** | **2** | **58,023** | **TR** | **28** |
| Q9Y3U8 | 60 S ribosomal protein L36 | 0.786 ± 0.001 | 2 | 12,303 | TR | 29 |
| **P62424** | **60 S ribosomal protein L7a** | **1.085 ± 0.096** | **3** | **30,148** | **TR** | **30** |
| P68133 | Actin, α skeletal muscle | 1.100 ± 0.054 | 14 | 42,366 | TR | 26 |
| **Q9HDC9** | **Adipocyte plasma membrane-associated protein** | **1.037 ± 0.120** | **8** | **46,622** | **TR** | **31** |
| **P07355** | **Annexin A2** | **1.095 ± 0.301** | **4** | **38,808** | **TR** | **28** |
| P24539 | ATP synthase B chain | 1.498 | 1 | 28,947 | TR | 29 |
| **P25705** | **ATP synthase subunit α** | **1.103 ± 0.101** | **21** | **59,828** | **TR** | **28** |
| **P06576** | **ATP synthase subunit β** | **1.099 ± 0.234** | **34** | **56,525** | **TR** | **29** |
| P53618 | Coatomer subunit β | 0.906 ± 0.054 | 4 | 108,214 | TR | 26 |
| Q9Y394 | Dehydrogenase/reductase SDR family member 7 precursor | 1.658 | 1 | 38,673 | TR | 31 |
| P54886 | $\Delta^1$-Pyrroline-5-carboxylate synthetase | 1.064 ± 0.151 | 3 | 87,989 | B | 32 |
| Q16531 | DNA damage-binding protein 1 | 1.224 ± 0.002 | 2 | 128,142 | TR | 28 |
| P39656 | Dolichyl-diphosphooligosaccharide-protein glycosyltransferase 48-kDa subunit precursor | 0.961 ± 0.125 | 8 | 48,893 | TR | 28 |
| P50402 | Emerin | 1.204 ± 0.137 | 4 | 29,033 | TR | 33 |
| **P15311** | **Ezrin (p81)** | **1.350 ± 0.029** | **2** | **69,484** | **TR** | **28** |
| Q06787 | Fragile X mental retardation 1 protein | 0.941 ± 0.006 | 2 | 71,473 | TR | 34 |
| **P62826** | **Androgen receptor-associated protein 24** | **1.259 ± 0.063** | **2** | **24,579** | **TR** | **28** |
| **P61978** | **Transformation up-regulated nuclear protein** | **1.095 ± 0.193** | **6** | **51,230** | **TR** | **32** |
| P52272 | Heterogeneous nuclear ribonucleoprotein M | 1.067 ± 0.060 | 5 | 77,749 | TR | 31 |
| **P05783** | **Keratin, type I cytoskeletal 18** | **1.100 ± 0.390** | **449** | **48,029** | **TR** | **28** |
| Q96AG4 | Leucine-rich repeat-containing protein 59 | 1.257 ± 0.337 | 5 | 35,308 | TR | 35 |
| Q08722 | Leukocyte surface antigen CD47 precursor | 1.957 | 1 | 35,590 | TR | 28 |
| **Q13724** | **Mannosyl-oligosaccharide glucosidase** | **0.980 ± 0.039** | **2** | **92,032** | **B** | **32** |
| P67812 | Microsomal signal peptidase 18-kDa subunit | 2.597 ± 0.298 | 2 | 20,612 | TR | 31 |
| Q8TCT9 | Signal peptide peptidase | 1.197 ± 0.153 | 2 | 41,747 | TR | 31 |
| Q9Y6C9 | Mitochondrial carrier homolog 2 | 0.671 ± 0.072 | 2 | 33,936 | TR | 29 |
| **P35580** | **Myosin heavy chain 10** | **1.333 ± 0.444** | **4** | **229,824** | **TR** | **28** |
| O94832 | Myosin-Id | 0.579 | 1 | 116,927 | TR | 29 |
| Q9Y2X3 | Nucleolar protein NOP5 | 1.632 ± 0.000 | 2 | 60,054 | TR | 36 |
| Q14160 | Protein LAP4 | 1.957 | 1 | 175,794 | TR | 29 |
| Q86UE4 | Astrocyte elevated gene 1 protein | 1.022 ± 0.046 | 4 | 63,856 | TR | 28 |
| **P46940** | **Ras GTPase-activating-like protein IQGAP1** | **0.994 ± 0.138** | **3** | **189,761** | **TR** | **31** |
| **P61026** | **Ras-related protein Rab-10** | **0.945 ± 0.148** | **7** | **22,755** | **TR** | **31** |
| Q14257 | E6-binding protein | 0.964 ± 0.017 | 3 | 36,911 | TR | 28 |
| Q9NW13 | RNA-binding protein 28 | 1.425 | 1 | 86,198 | TR | 31 |
| P05023 | Sodium/potassium-transporting ATPase α-1 chain precursor | 1.100 ± 0.130 | 17 | 114,135 | TR | 35 |
| P50991 | T-complex protein 1 subunit δ | 1.164 ± 0.124 | 2 | 58,401 | TR | 32 |
| Q5JTV8 | Torsin-1A-interacting protein 1 | 0.876 ± 0.002 | 2 | 66,379 | TR | 31 |
| Q15363 | Transmembrane emp24 domain-containing protein 2 precursor | 1.672 | 1 | 22,860 | TR | 28 |
| **P40939** | **Trifunctional enzyme subunit α** | **1.288 ± 0.407** | **8** | **83,688** | **TR** | **31** |
| Q9NYL9 | Tropomodulin-3 (ubiquitous tropomodulin) | 1.837 | 1 | 39,741 | TR | 37 |
| Q9NZB2 | UPF0318 protein FAM120A | 0.927 ± 0.083 | 3 | 117,711 | TR | 28 |
| Q96A26 | E2-induced gene 5 protein | 2.3 ± 0.1 | 2 | 17,559 | TR | 29 |

TABLE I—*continued*

| Swiss-Prot accession no. | Protein name | Mean ± S.D. | No. of peptides | Molecular mass | Comments | Refs. |
|---|---|---|---|---|---|---|
| | | | | *Da* | | |
| Q8WY22 | Cervical cancer 1 proto-oncogene-binding protein KG19 | 1.393 | 1 | 27,932 | TR | 38 |
| Q15005 | Signal peptidase complex subunit 2 | 1.315 ± 0.034 | 4 | 25,272 | TR | 28 |
| **3. Both ERα− and c-Myc-related** | | | | | | |
| **P63104** | **14-3-3 protein ζ/δ (protein kinase C inhibitor protein 1)** | **1.372** | **1** | **27,899** | **TR** | **26, 28** |
| **P09110** | **3-Ketoacyl-CoA thiolase** | **1.148 ± 0.018** | **2** | **44,834** | **TR** | **28, 39** |
| P62277 | 40 S ribosomal protein S13 | 1.042 ± 0.105 | 4 | 17,212 | TR | 26, 33 |
| **P62263** | **40 S ribosomal protein S14** | **1.180 ± 0.003** | **2** | **16,434** | **TR** | **28, 40** |
| **P62249** | **40 S ribosomal protein S16** | **1.211 ± 0.005** | **3** | **16,549** | **TR** | **33, 41** |
| P08708 | 40 S ribosomal protein S17 | 1.326 | 1 | 15,597 | TR | 26, 33 |
| P62269 | 40 S ribosomal protein S18 | 1.083 ± 0.137 | 2 | 17,708 | TR | 26, 30 |
| P61247 | 40 S ribosomal protein S3a | 1.038 ± 0.052 | 9 | 30,154 | TR | 26 |
| **P62753** | **Phosphoprotein NP33** | **1.174 ± 0.001** | **2** | **28,834** | **TR** | **26, 42** |
| **P62241** | **40 S ribosomal protein S8** | **1.271 ± 0.067** | **2** | **24,475** | **TR** | **26, 28** |
| **P10809** | **60-kDa heat shock protein** | **1.041 ± 0.108** | **8** | **61,187** | **TR** | **26, 43** |
| P62913 | 60 S ribosomal protein L11 | 1.292 ± 0.248 | 3 | 20,468 | TR | 26, 44 |
| P26373 | Breast basic conserved protein 1 | 1.020 ± 0.049 | 2 | 24,304 | TR | 26, 33 |
| **P46776** | **60 S ribosomal protein L27a** | **1.089 ± 0.082** | **2** | **16,665** | **TR** | **26, 45** |
| **Q02878** | **TAX-responsive enhancer element-binding protein 107** | **0.898 ± 0.001** | **2** | **32,765** | **TR** | **26, 33** |
| P18124 | 60 S ribosomal protein L7 | 1.062 ± 0.001 | 2 | 29,264 | TR | 26, 28 |
| P32969 | 60 S ribosomal protein L9 | 1.173 ± 0.138 | 4 | 21,964 | TR | 26, 33 |
| **P60709** | **Actin, cytoplasmic 1 (β-actin)** | **1.087 ± 0.107** | **24** | **42,052** | **B, TR** | **26, 46** |
| P05141 | ADP/ATP translocase 2 | 1.020 ± 0.221 | 5 | 33,102 | TR | 26, 28 |
| **P12956** | **Thyroid-lupus autoantigen (CTC box-binding factor 75-kDa subunit)** | **1.066 ± 0.298** | **4** | **70,084** | **B, TR** | **33, 40** |
| Q9NYF8 | Bcl-2-associated transcription factor 1 (Btf) | 1.177 ± 0.002 | 2 | 106,173 | **TR** | 23, 28 |
| **P27824** | **Calnexin precursor** | **1.187 ± 0.101** | **5** | **67,982** | **TR** | **26, 28** |
| O14976 | Cyclin G-associated kinase | 1.212 ± 0.153 | 2 | 144,583 | TR | 26, 33 |
| P04844 | Dolichyl-diphosphooligosaccharide | 1.045 ± 0.132 | 18 | 69,355 | B, TR | 26, 32 |
| **P49411** | **Elongation factor Tu** | **1.181 ± 0.491** | **6** | **49,852** | **TR** | **26, 28** |
| **P14625** | **Endoplasmin precursor** | **1.342** | **1** | **92,696** | **TR** | **33, 40** |
| Q92616 | GCN1-like protein 1 | 0.929 ± 0.049 | 4 | 294,953 | TR | 26, 35 |
| **P04406** | **Glyceraldehyde-3-phosphate dehydrogenase** | **1.113 ± 0.258** | **3** | **36,201** | **TR** | **28, 40** |
| **P11142** | **Heat shock cognate 71-kDa protein** | **1.029 ± 0.253** | **5** | **71,082** | **TR, B** | **42, 47** |
| **P07900** | **Heat shock protein HSP 90-α** | **1.088 ± 0.087** | **2** | **85,006** | **TR, B** | **28, 48** |
| **P08238** | **Heat shock protein HSP 90-β** | **1.029 ± 0.004** | **2** | **83,554** | **TR, B** | **28, 49** |
| **P09651** | **Heterogeneous nuclear ribonucleoprotein A1** | **1.069 ± 0.171** | **5** | **38,936** | **TR** | **40, 45** |
| P51991 | Heterogeneous nuclear ribonucleoprotein A3 | 1.008 ± 0.197 | 5 | 39,799 | TR | 35, 40 |
| P14866 | Heterogeneous nuclear ribonucleoprotein L | 0.998 ± 0.124 | 3 | 60,719 | TR | 29, 40 |
| **O60506** | **Heterogeneous nuclear ribonucleoprotein Q** | **1.374** | **1** | **69,788** | **TR** | **26, 28** |
| P07910 | Heterogeneous nuclear ribonucleoproteins C1/C2 | 1.096 ± 0.183 | 19 | 33,707 | TR | 35, 40 |
| P16401 | Histone H1.5 | 1.047 ± 0.160 | 8 | 22,566 | TR | 29, 40 |
| Q71UI9 | Histone H2AV | 1.067 ± 0.110 | 33 | 13,501 | TR | 26, 28 |
| P62807 | Histone H2B type 1-C/E/F/G/I | 1.170 ± 0.458 | 58 | 13,811 | TR | 33, 41 |
| Q16836 | Hydroxyacyl-coenzyme A dehydrogenase | 1.331 ± 0.178 | 2 | 34,313 | TR | 26, 28 |
| P08779 | Keratin, type I cytoskeletal 16 | 1.099 ± 0.379 | 25 | 51,578 | TR | 26 |
| Q96G23 | Tumor metastasis suppressor gene 1 protein | 0.971 ± 0.001 | 2 | 44,961 | TR | 25, 35 |
| P02545 | Lamin-A/C | 1.084 ± 0.144 | 9 | 74,380 | TR | 26, 42 |
| P20700 | Lamin-B1 | 1.204 ± 0.221 | 10 | 66,653 | TR | 26, 28 |
| Q16891 | Proliferation-inducing gene 4 protein | 1.033 ± 0.115 | 4 | 84,026 | TR | 26, 28 |
| **P60660** | **Myosin light polypeptide 6** | **1.272 ± 0.001** | **2** | **17,090** | **TR** | **26, 50** |
| **P35579** | **Myosin-9** | **0.966 ± 0.193** | **17** | **227,646** | **TR** | **31, 40** |
| O43795 | Myosin-Ib | 0.955 ± 0.108 | 3 | 132,928 | TR | 26, 51 |
| Q15758 | Neutral amino acid transporter B(0) | 1.098 ± 0.113 | 3 | 57,018 | TR | 26, 28 |
| **P06748** | **Nucleophosmin (NPM) (nucleolar phosphoprotein B23)** | **0.996 ± 0.019** | **4** | **32,726** | **TR** | **40, 43** |
| P26599 | Polypyrimidine tract-binding protein 1 | 1.020 ± 0.296 | 6 | 57,357 | TR | 28, 39 |
| **Q6P2Q9** | **Pre-mRNA processing-splicing factor 8** | **1.030 ± 0.092** | **4** | **274,738** | **B** | **40, 51** |
| P35232 | Prohibitin | 1.012 ± 0.147 | 7 | 29,843 | TR, B | 52, 53 |

TABLE I—*continued*

| Swiss-Prot accession no. | Protein name | Mean ± S.D. | No. of peptides | Molecular mass | Comments | Refs. |
|---|---|---|---|---|---|---|
| | | | | *Da* | | |
| Q99623 | Prohibitin-2 (repressor of estrogen receptor activity) | 1.144 ± 0.197 | 7 | 33,276 | TR, B | 33, 40 |
| **Q15084** | **Protein-disulfide isomerase A6 precursor** | **1.243 ± 0.027** | **2** | **48,490** | **TR** | **26, 28** |
| **Q9BSJ8** | **Protein FAM62A** | **0.982 ± 0.040** | **6** | **123,293** | **TR** | **26, 40** |
| O43143 | Putative pre-mRNA splicing factor ATP-dependent RNA helicase DHX15 | 1.558 | 1 | 91,673 | TR | 26, 32 |
| Q15050 | Ribosome biogenesis regulatory protein homolog | 1.322 | 1 | 41,225 | TR | 28, 54 |
| **Q9H3N1** | **Thioredoxin domain-containing protein 1 precursor** | **1.235 ± 0.222** | **2** | **32,170** | **TR** | **26, 35** |
| **Q13263** | **Transcription intermediary factor 1-β (nuclear corepressor KAP-1)** | **1.083 ± 0.094** | **2** | **90,261** | **TR, B** | **32, 40** |
| Q9UNL2 | Translocon-associated protein subunit γ (TRAP-γ) | 1.151 ± 0.001 | 2 | 21,067 | TR | 25, 35 |
| **P68363** | **Tubulin α ubiquitous chain** | **0.950 ± 0.271** | **103** | **50,804** | **B** | **28, 55** |
| **P07437** | **Tubulin β chain** | **1.015 ± 0.195** | **38** | **50,095** | **TR, B** | **26, 55** |
| **P68371** | **Tubulin β-2C chain** | **1.021 ± 0.186** | **39** | **50,255** | **TR** | **26** |
| Q9P0L0 | Vesicle-associated membrane protein-associated protein A | 0.921 ± 0.002 | 2 | 28,103 | TR | 26, 33 |
| O95292 | Vesicle-associated membrane protein-associated protein B/C | 0.921 ± 0.002 | 2 | 27,439 | TR | 26, 31 |
| **O75396** | **Vesicle-trafficking protein SEC22b** | **0.897 ± 0.022** | **2** | **24,896** | **TR** | **26, 31** |
| P21796 | Voltage-dependent anion-selective channel protein 1 | 1.168 ± 0.379 | 26 | 30,868 | TR | 26, 35 |
| Q9Y277 | Voltage-dependent anion-selective channel protein 3 | 1.045 ± 0.043 | 3 | 30,981 | TR | 26, 28 |
| **P68104** | **Elongation factor 1-α 1** | **1.159 ± 0.065** | **3** | **50,451** | **TR** | **26, 28** |
| O94972 | Tripartite motif-containing protein 37 | 1.882 | 1 | 109,491 | TR | |
| **P22626** | **Heterogeneous nuclear ribonucleoproteins A2/B1** | **1.032 ± 0.173** | **16** | **37,464** | **TR** | **33, 40** |
| P33778 | Histone H2B type 1-B | 1.177 ± 0.455 | 58 | 13,942 | TR | 29, 40 |
| P84243 | Histone H3.3 | 1.393 ± 1.100 | 28 | 15,376 | TR | 28, 40 |
| O75367 | Core histone macro-H2A.1 | 1.2 ± 0.4 | 8 | 39,764 | TR | 26, 33 |
| **4. Others** | | | | | | |
| **Q15008** | **Breast cancer-associated protein SGA-113 m** | **0.985 ± 0.112** | **6** | **45,787** | **—** | |
| Q16352 | α-Internexin (α-Inx) | 0.366 ± 0.068 | 6 | 55,528 | — | |
| P00403 | Cytochrome *c* oxidase subunit 2 | 0.983 ± 0.095 | 4 | 25,719 | — | |
| **P15924** | **Desmoplakin (DP)** | **1.008 ± 0.061** | **5** | **334,021** | **—** | **56** |
| Q14315 | Filamin-C | 2.728 | 1 | 293,344 | — | |
| P20671 | Histone H2A type 1 | 1.063 ± 0.200 | 47 | 14,099 | — | |
| Q71DI3 | Histone H3.2 | 0.970 ± 0.201 | 31 | 15,436 | — | |
| P62805 | Histone H4 | 1.004 ± 0.196 | 162 | 11,360 | — | 57 |
| **P04264** | **Keratin, type II cytoskeletal 1** | **0.987 ± 0.086** | **157** | **66,149** | **—** | **58** |
| P02538 | Keratin, type II cytoskeletal 6A | 1.215 ± 0.346 | 19 | 60,293 | — | 59 |
| **P05787** | **Keratin, type II cytoskeletal 8** | **1.072 ± 0.447** | **565** | **53,671** | **—** | **60** |
| **Q7Z406** | **Myosin-14** | **1.014 ± 0.208** | **4** | **228,889** | **—** | |
| P16435 | NADPH-cytochrome P450 reductase | 0.913 ± 0.000 | 2 | 77,097 | — | |
| Q9H0U4 | Ras-related protein Rab-1B | 1.149 ± 0.112 | 5 | 22,328 | — | |
| P62834 | Ras-related protein Rap-1A precursor | 0.956 ± 0.085 | 3 | 21,316 | — | 61 |
| Q96HR9 | Receptor expression-enhancing protein 6 | 1.004 ± 0.178 | 4 | 20,891 | — | 62 |
| O94901 | Sad1/unc-84 protein-like 1 | 1.180 ± 0.045 | 2 | 90,806 | — | |
| P04350 | Tubulin β-4 chain | 0.943 ± 0.153 | 17 | 50,010 | — | 63 |
| Q96CS3 | UBX domain-containing protein 8 | 0.998 ± 0.035 | 3 | 52,933 | — | 64 |

In addition, the AuNP probes fabricated here bear a high charge density on their surface and thus have good solubility and high stability in solutions with an ionic strength up to more than 2 M (in Supplemental Fig. S2). As displayed in Fig. 1*C*, except when centrifuged, AuNPs remain soluble and well suspended throughout the pulldown process regardless of the buffer exchange. Such advantage is superior to many other nanomaterials and is particularly useful for affinity capturing from a relatively large volume of dilute biological fluids up to several liters (16). Another unique advantage of using AuNPs as probes is the visual monitoring of the modification. In the presence of salts, monodispersed AuNPs with a red color normally indicate a very uniform and complete surface coating, which could be easily obtained by the use of thiolated SAM molecules for AuNPs. Unlike magnetic beads, however, precipitation by centrifugation is required for the AuNP probes to separate the supernatant from the pellet, and this process could

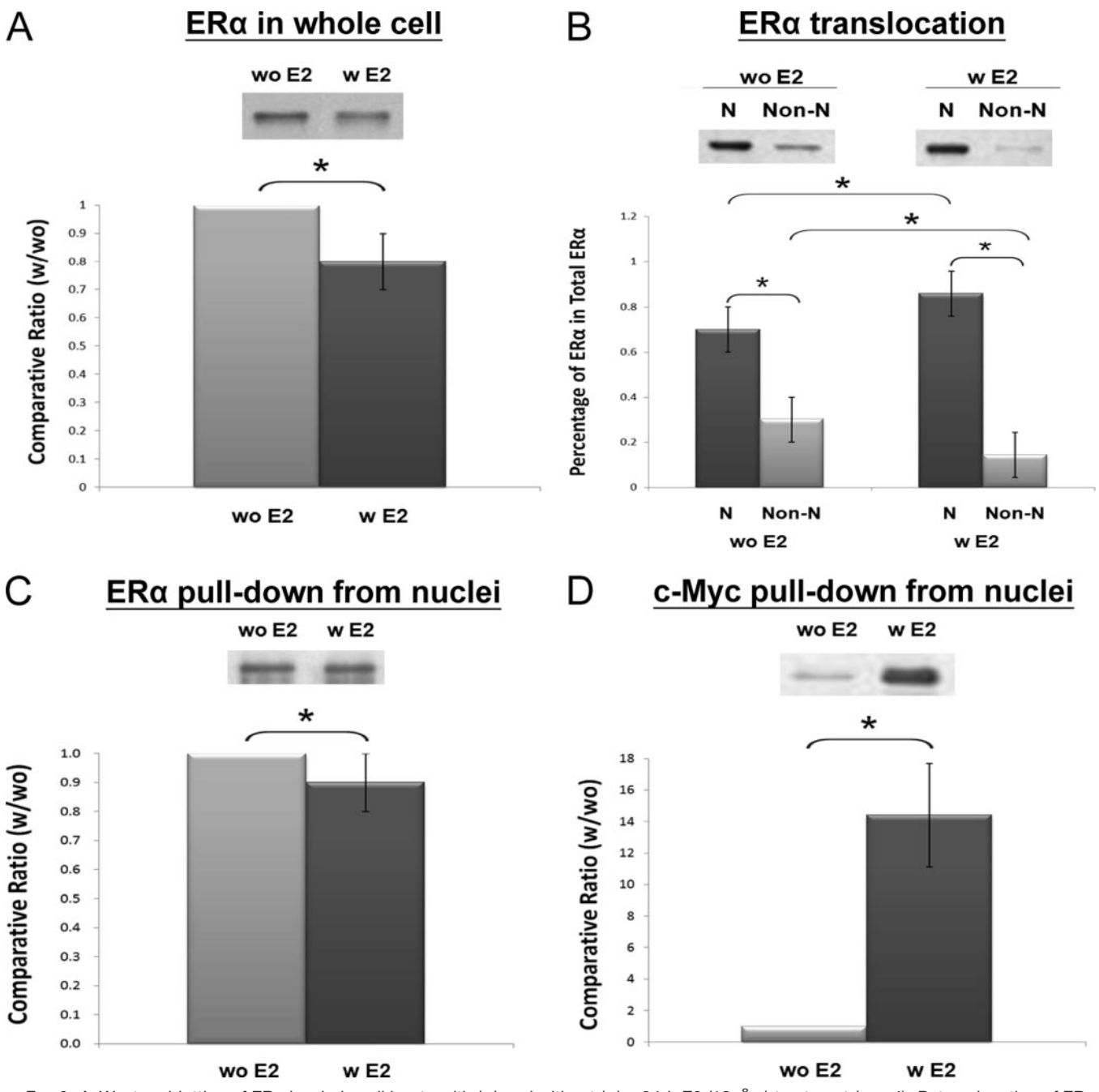


FIG. 6. *A*, Western blotting of ERα in whole cell lysate with (*w*) and without (*w*) a 24-h E2 ($10^{-8}$ M) treatment ($n = 4$). *B*, translocation of ERα from the non-nuclei (*non-N*) to the nuclei (*N*) of MCF-7 cells upon 24-h stimulation with E2 ($10^{-8}$ M) ($n = 8$). *C*, ERα in the AuNP-ERE pulldown from the nuclear fractions with and without E2 treatment ($n = 5$). *D*, c-Myc in the AuNP-ERE pulldown from the nuclear fractions with and without E2 treatment ($n = 3$). Significant differences ($p < 0.05$) are indicated with the *star* (*).

cause sample loss. We had tried to optimize the tubes, centrifugation speed and time, and the elution buffer for the purification. As shown in Fig. 2*A*, the recovery yield was estimated to be higher than 80% with 1% SDS elution.

Thus, we concluded that the AuNP-ERE probe exhibits good solubility, extremely low nonspecific binding, and comparable loading capacity, leading to a 20-fold enrichment of the factor compared with gel beads. We further concluded that chemically modified AuNPs exhibit excellent solubility and could become superior to magnetic beads if AuNPs can be more efficiently collected and separated from the supernatant, which, however, can be easily achieved by careful optimizations.

*Quantitative and Statistical Analysis in Revealing Specific/Nonspecific Binding*—As shown in the plot of Fig. 4*C*, more than 97% of the identified proteins have enrichment factors (ratios) greater than 1 (positive/negative), and about 72% of

the proteins (236 proteins) have enrichment factors large enough to indicate significant binding under 90% confidence, demonstrating a good specificity for the probe. In contrast, as shown in Fig. 4*D*, the average of all ratios with and without E2 treatment was around 0.9 for all pulled down proteins, and only about one-half of the proteins were found to change significantly under 75% confidence, indicating that small changes occur across proteins with a 24-h E2 treatment. We used a lower confidence level for Experiment 2 (75%) because ER$\alpha$ was reported to show maximal binding to the consensus sequence at 3 h after E2 treatment and return to near basal levels at the 12- and 24-h time periods based on chromatin immunoprecipitation-chip analysis (23). We used a lower confidence level to cover more potential proteins that may be involved in the transcription. Serum albumin is a well known, highly abundant protein that is commonly used as the blocking agent against nonspecific binding on solid supports and thus is a suitable control for quantitative analysis. In addition to the small difference in ratio values compared with the control, many discriminated proteins were due to few peptides used for quantification ($\leq$2). To increase the confidence of proteins identified and quantified by single peptides, we had used the unique dimethylated $a_1$ ion and relatively large cutoff values as the criteria. The identity and quantification ratio of AN32A and BZW1, which were identified by single peptides, were further confirmed by Western blotting. Thus, we believe the approach using PEG-modified AuNPs probes coupled with stable isotope dimethyl labeling and statistics could provide high confidence for specific binding as well as for protein identification and quantification.

*c-Myc and ER$\alpha$*—Based on quantification and statistics assessment, our data show that a total of 147 proteins (Table I) are regulated by E2 treatment. This large number of proteins reflects multiple pathways associated with E2 action. Notably, based on pathway analysis, a majority of affected proteins are involved in the transcriptional regulation of not only ER$\alpha$ but also c-Myc. Proteins regulated by both transcription factors account for 50% of all affected proteins, proteins regulated by only c-Myc account for 33%, and proteins regulated by only ER$\alpha$ account for 4%. Apparently, many more proteins are regulated by c-Myc than are regulated by ER$\alpha$. We believe such results were related to the dynamic change of the signaling and were consistent with the substantial E2-enhanced ERE binding for c-Myc and small changes in E2-enhanced ERE binding for ER$\alpha$ under a 24-h treatment. c-Myc is known to be encoded by estrogen-responsive proto-oncogenes (24), and the co-precipitation of ER$\alpha$ and c-Myc by the ERE probe revealed here is strong evidence of cross-interactions between the two transcription factors for ER-mediated transcription. It has been reported that the binding element of c-Myc is located in close proximity to the binding element of ER$\alpha$ in many estrogen-responsive promoters (23). Thus, E2 stimulation further enhances the interaction between c-Myc and ER$\alpha$ (23), facilitating the association of transcription factors and coactivators/repressors with these estrogen-responsive promoters. In addition to c-Myc, there were other transcription factors identified in the ERE complex but with insignificant changes by E2 stimulation after the 24-h time period. We suspect that these identified transcription factors could still be involved in ER-mediated transcription but that they become activated under different time periods of E2 stimulation.

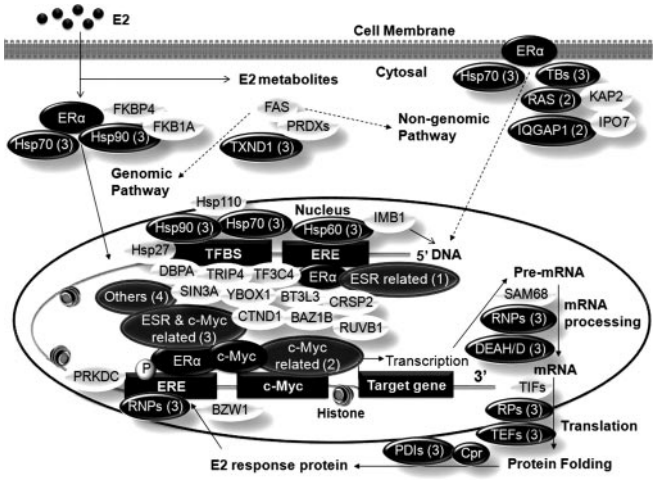


FIG. 7. **Proposed ERE complex consists of proteins classified in Table I as only ER$\alpha$-related (*1*), only c-Myc-related (*2*), both ER$\alpha$- and c-Myc-related (*3*), and others (*4*) and other identified proteins.** Proteins in *black ovals* are significantly affected by E2 stimulation, and proteins in *open ovals* are transcription factors identified from the pulldown but without significant changes induced by a 24-h E2 stimulation. *PRDXs*, peroxiredoxins PRDX1, PRDX2, PRDX3, and PRDX6; *TBs*, tubulin; *RAS*, Ras-related proteins; *RNPs*, ribonucleoprotein; *TIFs*, translation initiation factor; *TEFs*, translation elongation factor; *RPs*, ribosomal protein; *PDIs*, protein-disulfide isomerases; *Cpr*, chaperone; *BAZ1B*, bromodomain adjacent to zinc finger domain protein 1B; *BT3L3*, transcription factor BTF3 homolog 3; *CTND1*, catenin $\delta$-1; *TRIP4*, activating signal cointegrator 1; *CRSP2*, cofactor required for Sp1 transcriptional activation subunit 2; *DBPA*, DNA-binding protein A; *RUVB1*, RuvB-like 1; *SIN3A*, paired amphipathic helix protein Sin3a; *TF3C4*, general transcription factor 3C polypeptide 4; *YBOX1*, nuclease-sensitive element-binding protein 1; *TFBS*, transcription factor binding sites; ESR, ER$\alpha$; FAS, fatty acid synthase; PRKDC, DNA-dependent protein kinase catalytic subunit.

Thus, based on results of the experiment, we proposed a functional ERE complex (Fig. 7) composed of all E2-affected proteins and some transcription factors with no significant changes detected under a 24-h E2 treatment. In principle, our AuNP-ERE probe was primarily designed to investigate the genomic pathway induced by the primary affinity interaction between ER and ERE to form the ERE·ER complex. The ERE·ER complex recruits other proteins such as coactivators and corepressors, which co-regulate the transcription of downstream DNA into mRNA, as well as proteins, which affect cell functions. Thus, coactivators, corepressors, and proteins involved in transcription and translation were expected to be co-pulled down via secondary interactions. However, ERE probe could also pull down transcription factors that interact

with ER$\alpha$ or bind to sites close to ERE such as c-Myc and other transcriptional factor binding sites depicted in Fig. 7. E2 enhanced the interaction among binding proteins and facilitated the association of transcription factors and coactivators/repressors with these estrogen-responsive promoters, influencing chromatin remodeling and increased/decreased transcription. As indicated in Table I, 50% of the affected proteins were implicated in the transcriptional regulation of both ER$\alpha$ and c-Myc, suggesting that E2 stimulation stabilizes the ERE complex, which consists of co-regulators of both transcription factors, thereby permitting other signal transduction pathways to fine tune estrogen-mediated signaling networks. In addition to transcriptional regulation, other processes such as the non-genomic pathway, metabolism, and antioxidant effects are also linked to estrogen action and result in disruption of the cell cycle, apoptosis, DNA repair, and therefore tumor formation. Many proteins identified from the pulldown by the AuNP-ERE probe were also found to be involved in these processes (Fig. 7). We believe dynamic analyses with different time points will reveal more insights regarding cross-interactions and co-regulations of transcription factors as well as other signaling processes.

*Conclusions*—In this study, we demonstrated a successful QNanoPX platform that combines chemically modified AuNPs, quantitative proteomics, biostatistics, and bioinformatics to reveal protein·DNA complexes using an affinity purification method. The AuNP-ERE probe was composed of a short DNA sequence (13 bp) of ERE, but it was shown to be capable of pulling down a large complex that includes transcription factors and their co-regulators. Information gained from such an approach is very useful for understanding cross-interactions among signal transduction pathways. The method is superior to the traditional gel beads because of its substantially lower nonspecific binding and higher solubility, which result in a greatly enhanced enrichment factor. There are still highly abundant proteins that are co-pulled down nonspecifically, but it does not appear to alter the ability of AuNPs to capture interesting proteins, suggesting that further chemistry optimization is still needed. In conclusion, QNanoPX holds great promise for analyzing protein complexes *in vivo* and will be very useful for diverse applications in the interactome.

*Acknowledgments*—Pathway analyses and data mining were done using the system provided by the Bioinformatics Core for Genomic Medicine and Biotechnology Development at the National Cheng-Kung University, supported by National Science Council Grant NSC 97-3112-B-006-011.

* This work was supported by the Nature Science Division of the National Science Council in Taiwan under a research program for multidisciplinary collaboration (Grant NSC-98-2922-I-006-051).

S The on-line version of this article (available at http://www.mcponline.org) contains in Supplemental 1 Figs. S1–S6 and Table S1.

¶ To whom correspondence should be addressed. E-mail: shchen@mail.ncku.edu.tw.

REFERENCES

1. Santen, R. J., Song, R. X., Zhang, Z., Kumar, R., Jeng, M. H., Masamura, S., Yue, W., and Berstein, L. (2003) Adaptive hypersensitivity to estrogen: mechanism for superiority of aromatase inhibitors over selective estrogen receptor modulators for breast cancer treatment and prevention. *Endocr.-Relat. Cancer* **10,** 111–130
2. Lupu, R., and Menendez, J. A. (2006) Minireview: targeting fatty acid synthase in breast and endometrial cancer: an alternative to selective estrogen receptor modulators? *Endocrinology* **147,** 4056–4066
3. Zhu, Z., Boobis, A. R., and Edwards, R. J. (2008) Identification of estrogen-responsive proteins in MCF-7 human breast cancer cells using label-free quantitative proteomics. *Proteomics* **8,** 1987–2005
4. Malorni, L., Cacace, G., Cuccurullo, M., Pocsfalvi, G., Chambery, A., Farina, A., Di Maro, A., Parente, A., and Malorni, A. (2006) Proteomic analysis of MCF-7 breast cancer cell line exposed to mitogenic concentration of 17 beta-estradiol. *Proteomics* **6,** 5973–5982
5. Matsuoka, S., Ballif, B. A., Smogorzewska, A., McDonald, E. R., 3rd, Hurov, K. E., Luo, J., Bakalarski, C. E., Zhao, Z., Solimini, N., Lerenthal, Y., Shiloh, Y., Gygi, S. P., and Elledge, S. J. (2007) ATM and ATR substrate analysis reveals extensive protein networks responsive to DNA damage. *Science* **316,** 1160–1166
6. Ranish, J. A., Hahn, S., Lu, Y., Yi, E. C., Li, X. J., Eng, J., and Aebersold, R. (2004) Identification of TFB5, a new component of general transcription and DNA repair factor IIH. *Nat. Genet.* **36,** 707–713
7. Wepf, A., Glatter, T., Schmidt, A., Aebersold, R., and Gstaiger, M. (2009) Quantitative interaction proteomics using mass spectrometry. *Nat. Methods* **6,** 203–205
8. Liao, L., Park, S. K., Xu, T., Vanderklish, P., and Yates, J. R., 3rd (2008) Quantitative proteomic analysis of primary neurons reveals diverse changes in synaptic protein content in fmr1 knockout mice. *Proc. Natl. Acad. Sci. U.S.A.* **105,** 15281–15286
9. Boersema, P. J., Aye, T. T., van Veen, T. A., Heck, A. J., and Mohammed, S. (2008) Triplex protein quantification based on stable isotope labeling by peptide dimethylation applied to cell and tissue lysates. *Proteomics* **8,** 4624–4632
10. Schulze, W. X., and Mann, M. (2004) A novel proteomic screen for peptide-protein interactions. *J. Biol. Chem.* **279,** 10756–10764
11. Guerrero, C., Tagwerker, C., Kaiser, P., and Huang, L. (2006) An integrated mass spectrometry-based proteomic approach: quantitative analysis of tandem affinity-purified in vivo cross-linked protein complexes (QTAX) to decipher the 26 S proteasome-interacting network. *Mol. Cell. Proteomics* **5,** 366–378
12. Phizicky, E. M., and Fields, S. (1995) Protein-protein interactions: methods for detection and analysis. *Microbiol. Rev.* **59,** 94–123
13. Alber, F., Dokudovskaya, S., Veenhoff, L. M., Zhang, W., Kipper, J., Devos, D., Suprapto, A., Karni-Schmidt, O., Williams, R., Chait, B. T., Sali, A., and Rout, M. P. (2007) The molecular architecture of the nuclear pore complex. *Nature* **450,** 695–701
14. Cristea, I. M., Williams, R., Chait, B. T., and Rout, M. P. (2005) Fluorescent proteins as proteomic probes. *Mol. Cell. Proteomics* **4,** 1933–1941
15. Baron, R., Willner, B., and Willner, I. (2007) Biomolecule-nanoparticle hybrids as functional units for nanobiotechnology. *Chem. Commun.* 323–332
16. Wang, A., Wu, C. J., and Chen, S. H. (2006) Gold nanoparticle-assisted protein enrichment and electroelution for biological samples containing low protein concentrations: a prelude of gel electrophoresis. *J. Proteome Res.* **5,** 1488–1492
17. Thaxton, C. S., Georganopoulou, D. G., and Mirkin, C. A. (2006) Gold nanoparticle probes for the detection of nucleic acid targets. *Clin. Chim. Acta* **363,** 120–126
18. Aubin-Tam, M. E., and Hamad-Schifferli, K. (2008) Structure and function of nanoparticle-protein conjugates. *Biomed. Mater.* **3,** 034001
19. Hsu, J. L., Huang, S. Y., Chow, N. H., and Chen, S. H. (2003) Stable-isotope dimethyl labeling for quantitative proteomics. *Anal. Chem.* **75,** 6843–6852
20. Hsu, J. L., Huang, S. Y., Shiea, J. T., Huang, W. Y., and Chen, S. H. (2005) Beyond quantitative proteomics: Signal enhancement of the a(1) ion as a mass tag for peptide sequencing using dimethyl labeling. *J. Proteome Res.* **4,** 101–108
21. Hsu, J. L., Huang, S. Y., and Chen, S. H. (2006) Dimethyl multiplexed labeling combined with microcolumn separation and MS analysis for

time course study in proteomics. *Electrophoresis* **27,** 3652–3660
22. Harris, D. C. (2007) *Quantitative Chemical Analysis*, 7th Ed., p. 61, W. H. Freeman and Co., New York
23. Cheng, A. S., Jin, V. X., Fan, M., Smith, L. T., Liyanarachchi, S., Yan, P. S., Leu, Y. W., Chan, M. W., Plass, C., Nephew, K. P., Davuluri, R. V., and Huang, T. H. (2006) Combinatorial analysis of transcription factor partners reveals recruitment of c-MYC to estrogen receptor-alpha responsive promoters. *Mol. Cell* **21,** 393–404
24. Weisz, A., and Rosales, R. (1990) Identification of an estrogen response element upstream of the human c-Fos gene that binds the estrogen-receptor and the AP-1 transcription factor. *Nucleic Acids Res.* **18,** 5097–5106
25. Lin, C. Y., Vega, V. B., Thomsen, J. S., Zhang, T., Kong, S. L., Xie, M., Chiu, K. P., Lipovich, L., Barnett, D. H., Stossi, F., Yeo, A., George, J., Kuznetsov, V. A., Lee, Y. K., Charn, T. H., Palanisamy, N., Miller, L. D., Cheung, E., Katzenellenbogen, B. S., Ruan, Y., Bourque, G., Wei, C. L., and Liu, E. T. (2007) Whole-genome cartography of estrogen receptor alpha binding sites. *PLoS Genet.* **3,** e87
26. Mani, K. M., Lefebvre, C., Wang, K., Lim, W. K., Basso, K., Dalla-Favera, R., and Califano, A. (2008) A systems biology approach to prediction of oncogenes and molecular perturbation targets in B-cell lymphomas. *Mol. Syst. Biol.* **4,** 169–177
27. Kininis, M., Chen, B. S., Diehl, A. G., Isaacs, G. D., Zhang, T., Siepel, A. C., Clark, A. G., and Kraus, W. L. (2007) Genomic analyses of transcription factor binding, histone acetylation, and gene expression reveal mechanistically distinct classes of estrogen-regulated promoters. *Mol. Cell. Biol.* **27,** 5090–5104
28. Chen, Y., Blackwell, T. W., Chen, J., Gao, J., Lee, A. W., and States, D. J. (2007) Integration of genome and chromatin structure with gene expression profiles to predict c-MYC recognition site binding and function. *PLoS Comput. Biol.* **3,** e63
29. Chen, X., Xu, H., Yuan, P., Fang, F., Huss, M., Vega, V. B., Wong, E., Orlov, Y. L., Zhang, W., Jiang, J., Loh, Y. H., Yeo, H. C., Yeo, Z. X., Narang, V., Govindarajan, K. R., Leong, B., Shahab, A., Ruan, Y., Bourque, G., Sung, W. K., Clarke, N. D., Wei, C. L., and Ng, H. H. (2008) Integration of external signaling pathways with the core transcriptional network in embryonic stem cells. *Cell* **133,** 1106–1117
30. Palomero, T., Lim, W. K., Odom, D. T., Sulis, M. L., Real, P. J., Margolin, A., Barnes, K. C., O'Neil, J., Neuberg, D., Weng, A. P., Aster, J. C., Sigaux, F., Soulier, J., Look, A. T., Young, R. A., Califano, A., and Ferrando, A. A. (2006) NOTCH1 directly regulates c-MYC and activates a feed-forward-loop transcriptional network promoting leukemic cell growth. *Proc. Natl. Acad. Sci. U.S.A.* **103,** 18261–18266
31. Margolin, A. A., Palomero, T., Sumazin, P., Califano, A., Ferrando, A. A., and Stolovitzky, G. (2009) ChIP-on-chip significance analysis reveals large-scale binding and regulation by human transcription factor oncogenes. *Proc. Natl. Acad. Sci. U.S.A.* **106,** 244–249
32. Koch, H. B., Zhang, R., Verdoodt, B., Bailey, A., Zhang, C. D., Yates, J. R., 3rd, Menssen, A., and Hermeking, H. (2007) Large-scale identification of c-MYC-associated proteins using a combined TAP/MudPIT approach. *Cell Cycle* **6,** 205–217
33. Li, Z., Van Calcar, S., Qu, C., Cavenee, W. K., Zhang, M. Q., and Ren, B. (2003) A global transcriptional regulatory role for c-Myc in Burkitt's lymphoma cells. *Proc. Natl. Acad. Sci. U.S.A.* **100,** 8164–8169
34. Drouin, R., Angers, M., Dallaire, N., Rose, T. M., Khandjian, E. W., and Rousseau, F. (1997) Structural and functional characterization of the human FMR1 promoter reveals similarities with the hnRNP-A2 promoter region. *Hum. Mol. Genet.* **6,** 2051–2060
35. Zeller, K. I., Zhao, X., Lee, C. W., Chiu, K. P., Yao, F., Yustein, J. T., Ooi, H. S., Orlov, Y. L., Shahab, A., Yong, H. C., Fu, Y., Weng, Z., Kuznetsov, V. A., Sung, W. K., Ruan, Y., Dang, C. V., and Wei, C. L. (2006) Global mapping of c-Myc binding sites and target gene networks in human B cells. *Proc. Natl. Acad. Sci. U.S.A.* **103,** 17834–17839
36. Sridharan, R., Tchieu, J., Mason, M. J., Yachechko, R., Kuoy, E., Horvath, S., Zhou, Q., and Plath, K. (2009) Role of the murine reprogramming factors in the induction of pluripotency. *Cell* **136,** 364–377
37. Reymann, S., and Borlak, J. (2008) Transcription profiling of lung adenocarcinomas of c-myc-transgenic mice: identification of the c-myc regulatory gene network. *BMC Syst. Biol.* **2,** 46–66
38. Kim, J., Chu, J., Shen, X., Wang, J., and Orkin, S. H. (2008) An extended transcriptional network for pluripotency of embryonic stem cells. *Cell* **132,** 1049–1061
39. Gao, H., Fält, S., Sandelin, A., Gustafsson, J. A., and Dahlman-Wright, K. (2008) Genome-wide identification of estrogen receptor alpha-binding sites in mouse liver. *Mol. Endocrinol.* **22,** 10–22
40. Blanchette, M., Bataille, A. R., Chen, X., Poitras, C., Laganière, J., Lefèbvre, C., Deblois, G., Giguère, V., Ferretti, V., Bergeron, D., Coulombe, B., and Robert, F. O. (2006) Genome-wide computational prediction of transcriptional regulatory modules reveals new insights into human gene expression. *Genome Res.* **16,** 656–668
41. Jin, V. X., Leu, Y. W., Liyanarachchi, S., Sun, H., Fan, M., Nephew, K. P., Huang, T. H., and Davuluri, R. V. (2004) Identifying estrogen receptor alpha target genes using integrated computational genomics and chromatin immunoprecipitation microarray. *Nucleic Acids Res.* **32,** 6627–6635
42. Fernandez, P. C., Frank, S. R., Wang, L., Schroeder, M., Liu, S., Greene, J., Cocito, A., and Amati, B. (2003) Genomic targets of the human c-Myc protein. *Genes Dev.* **17,** 1115–1129
43. Zeller, K. I., Jegga, A. G., Aronow, B. J., O'Donnell, K. A., and Dang, C. V. (2003) An integrated database of genes responsive to the Myc oncogenic transcription factor: identification of direct genomic targets. *Genome Biol.* **4,** R69
44. Dai, M. S., and Lu, H. (2008) Crosstalk between c-Myc and ribosome in ribosomal biogenesis and cancer. *J. Cell. Biochem.* **105,** 670–677
45. Kim, J., Lee, J. H., and Iyer, V. R. (2008) Global identification of Myc target genes reveals its direct role in mitochondrial biogenesis and its E-box usage in vivo. *PLoS One* **3,** e1798
46. Park, J., Wood, M. A., and Cole, M. D. (2002) BAF53 forms distinct nuclear complexes and functions as a critical c-Myc-interacting nuclear cofactor for oncogenic transformation. *Mol. Cell. Biol.* **22,** 1307–1316
47. Ogawa, S., Oishi, H., Mezaki, Y., Kouzu-Fujita, M., Matsuyama, R., Nakagomi, M., Mori, E., Murayama, E., Nagasawa, H., Kitagawa, H., Yanagisawa, J., Yano, T., and Kato, S. (2005) Repressive domain of unliganded human estrogen receptor alpha associates with Hsc70. *Genes Cells* **10,** 1095–1102
48. Aumais, J. P., Lee, H. S., Lin, R., and White, J. H. (1997) Selective interaction of hsp90 with an estrogen receptor ligand-binding domain containing a point mutation. *J. Biol. Chem.* **272,** 12229–12235
49. Bouhouche-Chatelier, L., Chadli, A., and Catelli, M. G. (2001) The N-terminal adenosine triphosphate binding domain of Hsp90 is necessary and sufficient for interaction with estrogen receptor. *Cell Stress Chaperones* **6,** 297–305
50. Denger, S., Bähr-Ivacevic, T., Brand, H., Reid, G., Blake, J., Seifert, M., Lin, C. Y., May, K., Benes, V., Liu, E. T., and Gannon, F. (2008) Transcriptome profiling of estrogen-regulated genes in human primary osteoblasts reveals an osteoblast-specific regulation of the insulin-like growth factor binding protein 4 gene. *Mol. Endocrinol.* **22,** 361–379
51. Ewing, R. M., Chu, P., Elisma, F., Li, H., Taylor, P., Climie, S., McBroom-Cerajewski, L., Robinson, M. D., O'Connor, L., Li, M., Taylor, R., Dharsee, M., Ho, Y., Heilbut, A., Moore, L., Zhang, S., Ornatsky, O., Bukhman, Y. V., Ethier, M., Sheng, Y., Vasilescu, J., Abu-Farha, M., Lambert, J. P., Duewel, H. S., Stewart, I. I., Kuehl, B., Hogue, K., Colwill, K., Gladwish, K., Muskat, B., Kinach, R., Adams, S. L., Moran, M. F., Morin, G. B., Topaloglou, T., and Figeys, D. (2007) Large-scale mapping of human protein-protein interactions by mass spectrometry. *Mol. Syst. Biol.* **3,** 89–105
52. He, B., Feng, Q., Mukherjee, A., Lonard, D. M., DeMayo, F. J., Katzenellenbogen, B. S., Lydon, J. P., and O'Malley, B. W. (2008) A repressive role for prohibitin in estrogen signaling. *Mol. Endocrinol.* **22,** 344–360
53. O'Connell, B. C., Cheung, A. F., Simkevich, C. P., Tam, W., Ren, X., Mateyak, M. K., and Sedivy, J. M. (2003) A large scale genetic analysis of c-Myc-regulated gene expression patterns. *J. Biol. Chem.* **278,** 12563–12573
54. Carroll, J. S., Meyer, C. A., Song, J., Li, W., Geistlinger, T. R., Eeckhoute, J., Brodsky, A. S., Keeton, E. K., Fertuck, K. C., Hall, G. F., Wang, Q., Bekiranov, S., Sementchenko, V., Fox, E. A., Silver, P. A., Gingeras, T. R., Liu, X. S., and Brown, M. (2006) Genome-wide analysis of estrogen receptor binding sites. *Nat. Genet.* **38,** 1289–1297
55. Azuma, K., Horie, K., Inoue, S., Ouchi, Y., and Sakai, R. (2004) Analysis of estrogen receptor alpha signaling complex at the plasma membrane. *FEBS Lett.* **577,** 339–344
56. Garrod, D., and Chidgey, M. (2008) Desmosome structure, composition

and function. *Biochim. Biophys. Acta* **1778,** 572–587
57. Friend, K., Lovejoy, A. F., and Steitz, J. A. (2007) U2 snRNP binds intronless histone pre-mRNAs to facilitate U7-snRN-dependent 3′ end formation. *Mol. Cell* **28,** 240–252
58. Meng, X., Krokhin, O., Cheng, K., Ens, W., and Wilkins, J. A. (2007) Characterization of IQGAP1-containing complexes in NK-like cells: evidence for Rac 2 and RACK1 association during homotypic adhesion. *J. Proteome Res.* **6,** 744–750
59. Rual, J. F., Venkatesan, K., Hao, T., Hirozane-Kishikawa, T., Dricot, A., Li, N., Berriz, G. F., Gibbons, F. D., Dreze, M., Ayivi-Guedehoussou, N., Klitgord, N., Simon, C., Boxem, M., Milstein, S., Rosenberg, J., Goldberg, D. S., Zhang, L. V., Wong, S. L., Franklin, G., Li, S., Albala, J. S., Lim, J., Fraughton, C., Llamosas, E., Cevik, S., Bex, C., Lamesch, P., Sikorski, R. S., Vandenhaute, J., Zoghbi, H. Y., Smolyar, A., Bosak, S., Sequerra, R., Doucette-Stamm, L., Cusick, M. E., Hill, D. E., Roth, F. P., and Vidal, M. (2005) Towards a proteome-scale map of the human protein-protein interaction network. *Nature* **437,** 1173–1178
60. Bouwmeester, T., Bauch, A., Ruffner, H., Angrand, P. O., Bergamini, G., Croughton, K., Cruciat, C., Eberhard, D., Gagneur, J., Ghidelli, S., Hopf, C., Huhse, B., Mangano, R., Michon, A. M., Schirle, M., Schlegl, J., Schwab, M., Stein, M. A., Bauer, A., Casari, G., Drewes, G., Gavin, A. C., Jackson, D. B., Joberty, G., Neubauer, G., Rick, J., Kuster, B., and Superti-Furga, G. (2004) A physical and functional map of the human TNF-alpha NF-kappa B signal transduction pathway. *Nat. Cell Biol.* **6,** 97–105
61. Jeong, H. W., Li, Z., Brown, M. D., and Sacks, D. B. (2007) IQGAP1 binds Rap1 and modulates its activity. *J. Biol. Chem.* **282,** 20752–20762
62. Meek, S. E., Lane, W. S., and Piwnica-Worms, H. (2004) Comprehensive proteomic analysis of interphase and mitotic 14-3-3-binding proteins. *J. Biol. Chem.* **279,** 32046–32054
63. Vladimirova, N. M., Murav'eva, T. I., Ovchinnikova, T. V., Potapenko, N. A., and Khodova, O. M. (1998) Na+,K+-ATPase isozymes in the bovine brain grey matter and stem. *Membr. Cell Biol.* **12,** 435–439
64. Alexandru, G., Graumann, J., Smith, G. T., Kolawa, N. J., Fang, R., and Deshaies, R. J. (2008) UBXD7 binds multiple ubiquitin ligases and implicates p97 in HIF1 alpha turnover. *Cell* **134,** 804–816